Report

Cell Reports

RbAp46/48^{LIN-53} Is Required for Holocentromere Assembly in *Caenorhabditis elegans*

Graphical Abstract

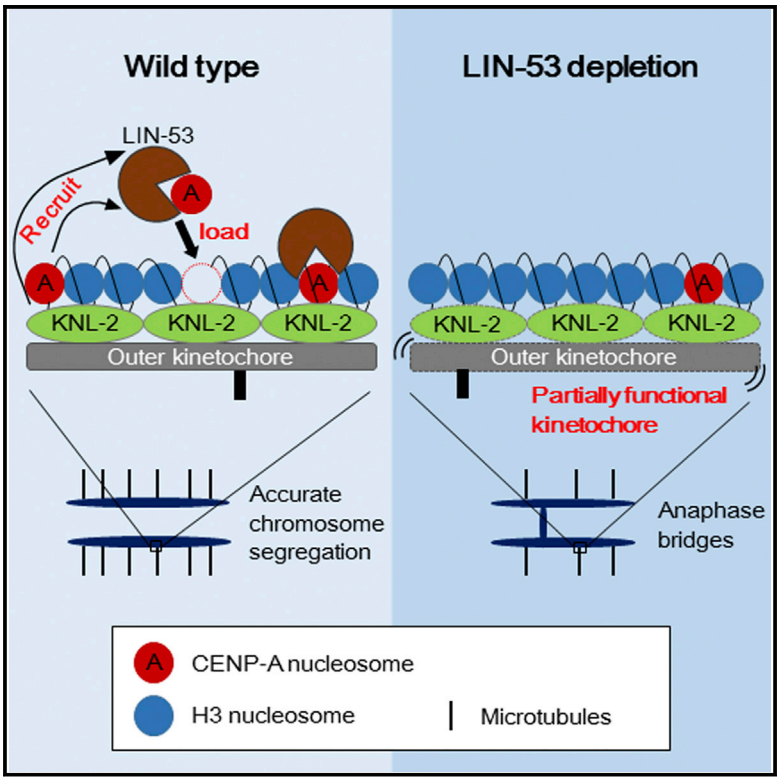

Highlights

- RbAp46/48^{LIN-53} is crucial for chromosome segregation in holocentric *C. elegans*
- RbAp46/48^{LIN-53} localizes to centromeres in metaphase and disappears in anaphase
- RbAp46/48^{LIN-53} localizes and stabilizes CENP-A^{HCP-3} for holocentromere assembly
- RbAp46/48^{LIN-53}'s centromeric role is not due to histone acetylation or methylation

Authors

Bernard Chi Hang Lee, Zhongyang Lin, Karen Wing Yee Yuen

Correspondence

kwyyuen@hku.hk

In Brief

Histone H3 variant CENP-A epigenetically marks all functional centromeres, but how it is assembled on holocentromeres is unknown. Lee et al. show that the histone chaperone RbAp46/48^{LIN-53} is required for CENP-A^{HCP-3} localization and accurate chromosome segregation in holocentric *C. elegans*. RbAp46/48^{LIN-53} may function to escort CENP-A^{HCP-3} for holocentromere assembly.

Lee et al., 2016, Cell Reports *14*, 1819–1828
March 1, 2016
http://dx.doi.org/10.1016/j.celrep.2016.01.065

Cell Reports
Report

RbAp46/48^{LIN-53} Is Required for Holocentromere Assembly in *Caenorhabditis elegans*

Bernard Chi Hang Lee,[1] Zhongyang Lin,[1] and Karen Wing Yee Yuen[1,*]
[1]School of Biological Sciences, the University of Hong Kong, Kadoorie Biological Sciences Building, Pokfulam Road, Hong Kong
*Correspondence: kwyyuen@hku.hk
http://dx.doi.org/10.1016/j.celrep.2016.01.065

SUMMARY

Centromeres, the specialized chromosomal regions for recruiting kinetochores and directing chromosome segregation, are epigenetically marked by a centromeric histone H3 variant, CENP-A. To maintain centromere identity through cell cycles, CENP-A diluted during DNA replication is replenished. The licensing factor M18BP1^{KNL-2} is known to recruit CENP-A to holocentromeres. Here, we show that RbAp46/48^{LIN-53}, a conserved histone chaperone, is required for CENP-A^{HCP-3} localization in holocentric *Caenorhabditis elegans*. Indeed, RbAp46/48^{LIN-53} and CENP-A^{HCP-3} localizations are interdependent. RbAp46/48^{LIN-53} localizes to the centromere during metaphase in a CENP-A^{HCP-3}- and M18BP1^{KNL-2}-dependent manner, suggesting CENP-A^{HCP-3} loading may occur before anaphase. RbAp46/48^{LIN-53} does not function at the centromere through histone acetylation, H3K27 trimethylation, or its known chromatin-modifying complexes. RbAp46/48^{LIN-53} may function independently to escort CENP-A^{HCP-3} for holocentromere assembly but is dispensable for other kinetochore protein recruitment. Nonetheless, depletion of RbAp46/48^{LIN-53} leads to anaphase bridges and chromosome missegregation. This study unravels the holocentromere assembly hierarchy and its conservation with monocentromeres.

INTRODUCTION

The centromere is the specialized chromatin domain responsible for recruiting the kinetochore, which directs chromosome segregation by interacting with spindle microtubules. The majority of centromeric chromatin is epigenetically marked by a conserved histone H3 variant, centromere protein A (CENP-A/CenH3). In each cell cycle, new CENP-A is deposited onto centromeric chromatin to replenish CENP-A diluted during DNA replication (Jansen et al., 2007; Shelby et al., 2000). A CENP-A-specific chaperone, Holliday-junction-recognizing protein (HJURP) in humans or Scm3 in budding and fission yeast, is responsible for the escort and assembly of CENP-A (Camahort et al., 2007; Mizuguchi et al., 2007; Williams et al., 2009; Pidoux et al., 2009; Foltz et al., 2009; Dunleavy et al., 2009).

The centromeric chromatin is proposed to be licensed to favor CENP-A assembly. In humans, Mis18 complex (Mis18α and β and M18BP1) is required for HJURP and CENP-A centromeric localization (Fujita et al., 2007; Barnhart et al., 2011). Human Mis18 complex localizes to the centromere from late anaphase to early G1, just prior to CENP-A deposition (Fujita et al., 2007). The centromeric localization of M18BP1 is regulated by its cell-cycle-dependent phosphorylation (Silva et al., 2012; McKinley and Cheeseman, 2014). M18BP1 in *Xenopus* and mouse cells is recruited by CENP-C, an inner kinetochore protein that itself requires CENP-A for its localization (Dambacher et al., 2012; Moree et al., 2011). This positive feedback loop provides a self-targeting mechanism for CENP-A.

In *S. pombe* and human cells, Mis18 complex physically interacts with RbAp46/48^{Mis16}, a WD40 repeat-containing histone chaperone associated with multiple chromatin-modifying complexes (Hayashi et al., 2004; Ai and Parthun, 2004; Kuzmichev et al., 2002; Müller et al., 2002; Parthun et al., 1996; Harrison et al., 2006; Hassig et al., 1997; Martínez-Balbás et al., 1998; Verreault et al., 1996, 1998; Xue et al., 1998). RbAp46/48^{Mis16} is required for CENP-A recruitment in *S. pombe*, humans, and *Drosophila* (Fujita et al., 2007; Furuyama et al., 2006; Hayashi et al., 2004). In *S. pombe*, RbAp46/48^{Mis16} and Mis18 maintained histone H3 and H4 at the centromere in a hypoacetylated state (Hayashi et al., 2004). By contrast, a histone deacetylase inhibitor rescued the CENP-A recruitment defect in Mis18α-depleted human cells (Fujita et al., 2007), suggesting that centromeric histones acetylation is crucial for centromere licensing. In *Drosophila*, RbAp48^{p55} on its own assembles CENP-A^{CID} chromatin in vitro by interacting with CENP-A^{CID} and H4 (Furuyama et al., 2006).

Although the kinetochore architecture is well conserved between monocentromeres and holocentromeres, it is unclear whether the centromere assembly pathway is conserved. In holocentric *C. elegans*, M18BP1^{KNL-2} is the only factor known for CENP-A^{HCP-3} centromeric localization (Maddox et al., 2007), and no homologs of Mis18 or HJURP^{Scm3} have been identified. M18BP1^{KNL-2} physically interacts with CENP-A^{HCP-3} and localizes at the centromere throughout the cell cycle (Maddox et al., 2007). Unlike in monocentric organisms, in which M18BP1 is upstream of CENP-A, M18BP1^{KNL-2} and CENP-A^{HCP-3} are interdependent for centromeric localization in *C. elegans*. Yet, the mechanistic details of CENP-A^{HCP-3} and M18BP1^{KNL-2} centromeric recruitment remain unclear. In addition, the deposition

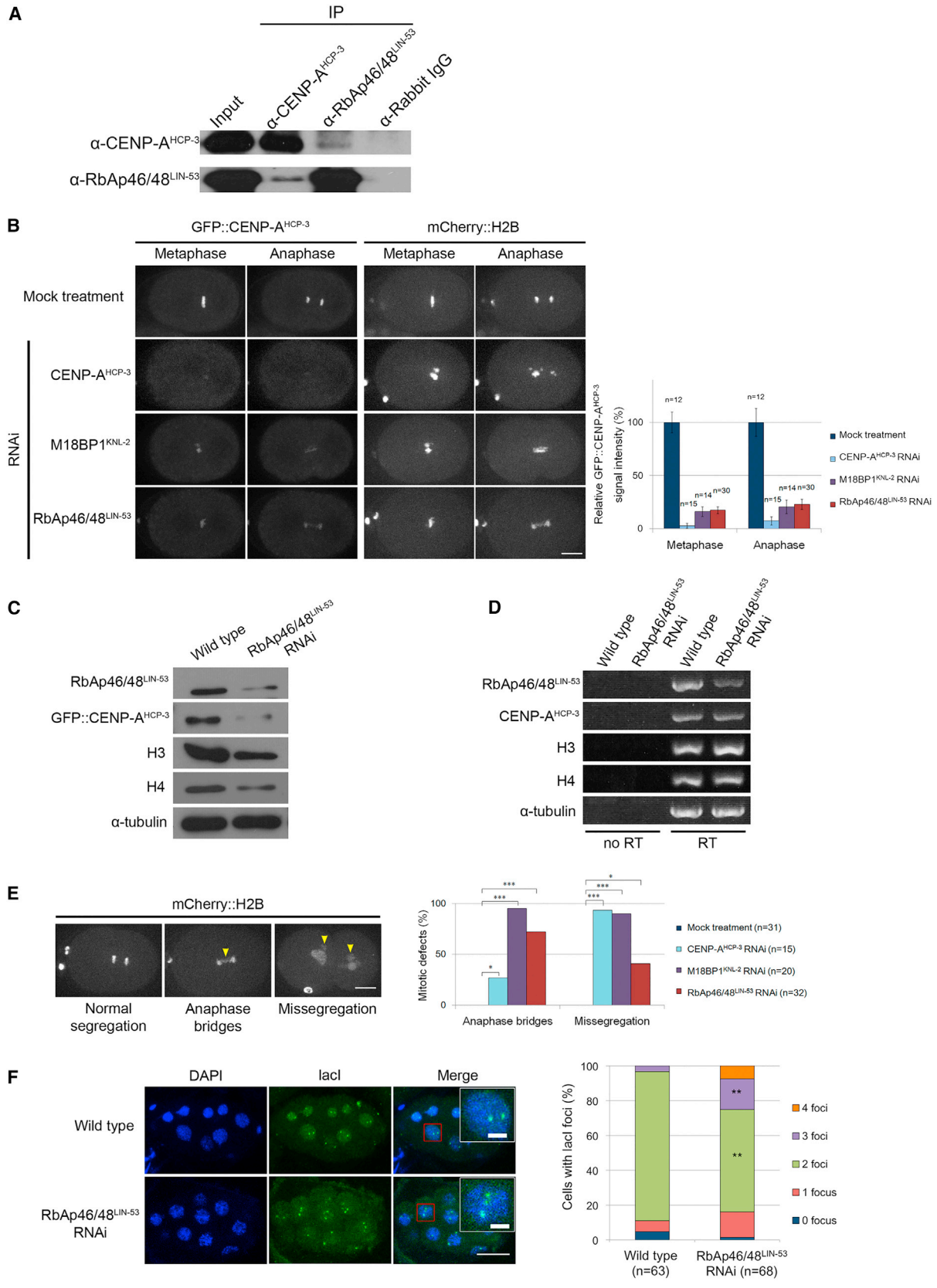

(legend on next page)

timing of new CNEP-A^{HCP-3} in the cell cycle remains unknown in *C. elegans*, unlike in humans, *Xenopus*, and yeast (Bernad et al., 2011; Jansen et al., 2007; Moree et al., 2011; Pearson et al., 2004; Takayama et al., 2008).

The dearth of knowledge on holocentromere assembly prompted us to search for CENP-A^{HCP-3}-interacting proteins that may be involved in CENP-A^{HCP-3} deposition. Using a proteomic approach in *C. elegans*, we identified the histone chaperone RbAp46/48^{LIN-53} as a CENP-A^{HCP-3}-associated protein. RbAp46/48^{LIN-53} was characterized as an antagonizing regulator of the Ras-signaling pathway for vulval induction (Lu and Horvitz, 1998) and a barrier for cellular reprogramming (Tursun et al., 2011). Here, we demonstrated that RbAp46/48^{LIN-53} is required for CENP-A^{HCP-3} centromeric recruitment and error-free chromosome segregation. We determined the localization dependencies between RbAp46/48^{LIN-53}, CENP-A^{HCP-3}, and M18BP1^{KNL-2}. We found that the function of RbAp46/48^{LIN-53} in CENP-A^{HCP-3} assembly is independent of its role in histone acetylation or H3K27 trimethylation as part of those known chromatin-modifying complexes. Our analysis on this new role of RbAp46/48^{LIN-53} in *C. elegans* contributes to our understanding of holocentromere assembly.

RESULTS

RbAp46/48^{LIN-53} Is Required for CENP-A^{HCP-3} Localization at Centromeres

To identify proteins potentially involved in CENP-A^{HCP-3} deposition at centromeres, we performed micrococcal nuclease digestion to isolate nucleosomes from *C. elegans* embryos and immunoprecipitated CENP-A^{HCP-3}. Mass spectrometric analysis identified the conserved histone chaperone, RbAp46/48^{LIN-53}, as a protein associated with CENP-A^{HCP-3} chromatin (Table S1). Reciprocal co-immunoprecipitation confirmed that CENP-A^{HCP-3} physically interacts with RbAp46/48^{LIN-53} (Figures 1A and S2A). To determine whether RbAp46/48^{LIN-53} is required for CENP-A^{HCP-3} centromeric localization, we depleted RbAp46/48^{LIN-53} by RNAi in CENP-A^{HCP-3} deletion mutant animals expressing GFP::CENP-A^{HCP-3} under the endogenous promoter. The animals also expressed mCherry::H2B for the visualization of chromosomes. Live-cell imaging of one-cell embryos showed that depletion of RbAp46/48^{LIN-53} removed the majority of CENP-A^{HCP-3} from mitotic chromosomes (Figures 1B, S1A, and S1B; Movie S1), similar to the effect of depleting M18BP1^{KNL-2} (Maddox et al., 2007). Consistently, immunofluorescence signal of centromeric CENP-A^{HCP-3} was lost upon RbAp46/48^{LIN-53} depletion (Figure S1C). To confirm RbAp46/48^{LIN-53} knockdown in protein and mRNA levels, western blot and RT-PCR were performed, respectively (Figures 1C, 1D, and S2B). To determine whether RbAp46/48^{LIN-53} and M18BP1^{KNL-2} function in the same CENP-A^{HCP-3} assembly pathway, we co-depleted RbAp46/48^{LIN-53} and M18BP1^{KNL-2} and found that the delocalization of CENP-A^{HCP-3} in the double depletion was similar to that of either single depletion (Figure S1B). The absence of a synergistic effect suggests that they function in the same pathway.

RbAp46/48^{LIN-53} Is Required for CENP-A^{HCP-3} Stability

Histones that fail to assemble on chromatin may be destabilized and degraded more easily. To determine whether the protein stability of CENP-A^{HCP-3} and other histones are affected by RbAp46/48^{LIN-53}, we performed western blot after RbAp46/48^{LIN-53} depletion. CENP-A^{HCP-3} and H4 protein levels were reduced significantly in RbAp46/48^{LIN-53} RNAi, whereas H3 and mCherry::H2B protein levels were reduced to a lesser degree (Figures 1C and S1D). To confirm that the effect of RbAp46/48^{LIN-53} RNAi on CENP-A^{HCP-3} is not via mRNA regulation, we showed by RT-PCR that CENP-A^{HCP-3} mRNA level did not change after RbAp46/48^{LIN-53} RNAi (Figure 1D). Our results suggest that RbAp46/48^{LIN-53} recruits and stabilizes CENP-A^{HCP-3} to holocentromeres. When transgenic GFP::CENP-A^{HCP-3} was expressed in the presence of endogenous CENP-A^{HCP-3}, the overall level of CENP-A^{HCP-3} was higher than in wild-type. However, such CENP-A^{HCP-3} overexpression did not rescue CENP-A^{HCP-3} delocalization upon RbAp46/48^{LIN-53} RNAi (Figures S1E and S1F), suggesting the main function of RbAp46/48^{LIN-53} lies in CENP-A^{HCP-3} localization, whereas CENP-A^{HCP-3} stabilization may be a secondary function.

Figure 1. RbAp46/48^{LIN-53} Depletion Delocalizes CENP-A^{HCP-3} from Mitotic Chromosomes and Causes Mitotic Defects

(A) Reciprocal co-immunoprecipitation of CENP-A^{HCP-3} and RbAp46/48^{LIN-53} using wild-type embryo extracts. Rabbit IgG immunoprecipitation (IP) was used as a negative control. Inputs and immunoprecipitates were analyzed by western blot.

(B) GFP::CENP-A^{HCP-3} and mCherry::H2B localization on metaphase and anaphase chromosomes in one-cell embryos by live-cell imaging following mock treatment, CENP-A^{HCP-3}, M18BP1^{KNL-2}, and RbAp46/48^{LIN-53} RNAi (Movie S1). CENP-A^{HCP-3} RNAi served as a positive control. The scale bar represents 10 μm. Quantification of GFP::CENP-A^{HCP-3} signal intensity on mitotic chromosomes in CENP-A^{HCP-3}, M18BP1^{KNL-2}, and RbAp46/48^{LIN-53} RNAi relative to mock treatment is shown. Error bars represent 95% confidence interval (CI) of the SEM.

(C) Western blot analysis of RbAp46/48^{LIN-53}, GFP::CENP-A^{HCP-3}, H3, and H4 protein levels in wild-type and RbAp46/48^{LIN-53}-depleted whole worms. α-tubulin was used as a loading control.

(D) RT-PCR analysis of RbAp46/48^{LIN-53}, CENP-A^{HCP-3}, H3, and H4 mRNA levels in wild-type and RbAp46/48^{LIN-53}-depleted whole worms. α-tubulin was used as a loading control.

(E) Representative images of normal chromosome segregation, anaphase bridges, and chromosome missegregation as indicated by chromatin marker mCherry::H2B in one-cell embryos by live-cell imaging. Anaphase bridges are indicated by lagging chromatin threads between separating sister chromatids, whereas chromosome missegregation refers to the presence of unequal or multiple chromatin masses at telophase (yellow arrowheads). The scale bar represents 10 μm. Quantification of the percentage of cells with the respective mitotic defects in mock treatment, CENP-A^{HCP-3}, M18BP1^{KNL-2}, or RbAp46/48^{LIN-53} RNAi. Chi-square test was used to test significance. *$p < 0.05$; ***$p < 0.0001$.

(F) Immunofluorescence staining of LacI, which binds to lacO integrated on translocated chromosome III/IV, and the chromatin (DAPI) in 8- to 16-cell embryos in wild-type and RbAp46/48^{LIN-53} RNAi. The scale bar represents 10 μm. Enlarged insets show the representative cells in red squares. The inset scale bar represents 2 μm. Quantification of the percentage of cells with zero to four LacI foci in wild-type and RbAp46/48^{LIN-53} RNAi is shown. Chi-square test was used to test significance. **$p < 0.01$.

See also Figures S1 and S2 and Movie S1.

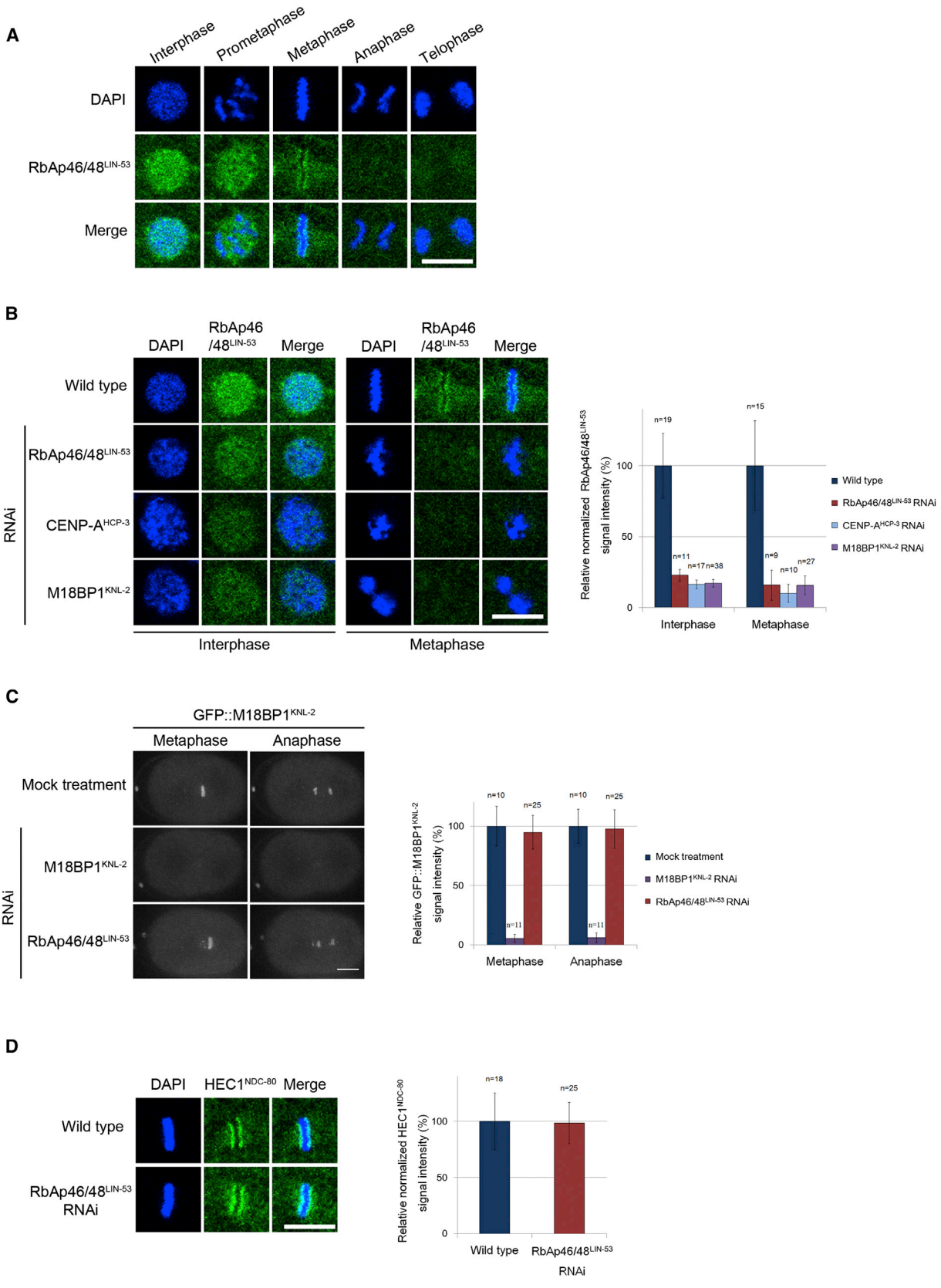

(legend on next page)

RbAp46/48^{LIN-53} Is Required for Accurate Chromosome Segregation

To investigate the function of RbAp46/48^{LIN-53} in chromosome segregation, we performed live-cell imaging in one-cell embryos expressing mCherry::H2B to monitor chromosome dynamics. Anaphase bridges were observed occasionally upon CENP-A^{HCP-3} depletion (27%) because chromosomes did not align before separation, whereas 95% of M18BP1^{KNL-2}-depleted cells exhibited anaphase bridges (Figure 1E). High rates of chromosome missegregation were observed after depletion of CENP-A^{HCP-3} (93%) or M18BP1^{KNL-2} (90%). When RbAp46/48^{LIN-53} was depleted, the metaphase plate could still be observed, yet 72% of one-cell embryos contain anaphase bridges and 41% undergo chromosome missegregation, both significantly higher than those in the mock treatment (Figure 1E).

To determine the degree of aneuploidy in multicellular embryos after depletion of RbAp46/48^{LIN-53}, we visualized lac operator (lacO) sequences integrated on a translocated chromosome through GFP-tagged lac repressor (lacI) binding (Figures 1F and S1G). Wild-type diploid embryos, as expected, contained mostly cells with two lacI foci (86%). By contrast, only 59% of cells in RbAp46/48^{LIN-53}-depleted embryos contained two lacI foci and 24% of cells contained three or more foci, indicating a significant degree of aneuploidy. Chromosome missegregation and aneuploidy after RbAp46/48^{LIN-53} depletion is expected to contribute to embryonic lethality (Figure S1A).

RbAp46/48^{LIN-53} Localizes at the Centromere in Metaphase in a CENP-A^{HCP-3}- and M18BP1^{KNL-2}-Dependent Manner

CENP-A^{HCP-3} and M18BP1^{KNL-2} localize at the centromere throughout the cell cycle in *C. elegans*, appearing as punctate foci in the nucleus in interphase and as continuous lines on the poleward faces of mitotic chromosomes (Maddox et al., 2007). To elucidate the time of action of RbAp46/48^{LIN-53} and its role in the centromere assembly hierarchy, we used immunofluorescence to investigate the localization of RbAp46/48^{LIN-53} and determine the localization dependency relationships with other centromeric proteins. RbAp46/48^{LIN-53} localized to the nucleus in interphase, was present at the centromere in metaphase, and was undetectable in anaphase and telophase (Figures 2A and S2C–S2E).

CENP-A^{HCP-3} and M18BP1^{KNL-2} are dependent on each other for centromeric localization and are at the top of the kinetochore assembly hierarchy (Maddox et al., 2007; Kitagawa, 2009). To determine whether the localization of RbAp46/48^{LIN-53} also depends on CENP-A^{HCP-3} and M18BP1^{KNL-2}, we performed immunofluorescence for RbAp46/48^{LIN-53} after CENP-A^{HCP-3} or M18BP1^{KNL-2} depletion. Both the nuclear and centromeric localization of RbAp46/48^{LIN-53} were reduced after CENP-A^{HCP-3} or M18BP1^{KNL-2} RNAi (Figure 2B), demonstrating that RbAp46/48^{LIN-53} localization to chromosomes is CENP-A^{HCP-3} and M18BP1^{KNL-2} dependent. These results, together with Figure 1B, show that RbAp46/48^{LIN-53} and CENP-A^{HCP-3} are interdependent on each other for localization.

RbAp46/48^{LIN-53} Is Not Required for Kinetochore Protein Recruitment

Having established that the localization of RbAp46/48^{LIN-53} was dependent on M18BP1^{KNL-2} (Figure 2B), we tested whether RbAp46/48^{LIN-53} in turn affected M18BP1^{KNL-2} localization. Live-cell imaging of one-cell embryos expressing GFP::M18BP1^{KNL-2} and immunostaining of endogenous M18BP1^{KNL-2} showed that M18BP1^{KNL-2} retained its centromeric localization after RbAp46/48^{LIN-53} depletion (Figures 2C and S2F–S2H).

As the centromeric localization of inner kinetochore protein M18BP1^{KNL-2} is independent of RbAp46/48^{LIN-53}, we investigated whether the localization of other kinetochore proteins was also independent of RbAp46/48^{LIN-53}. Immunostaining of outer kinetochore protein HEC1^{NDC-80} showed that HEC1^{NDC-80} still localized to kinetochores in metaphase after RbAp46/48^{LIN-53} depletion (Figure 2D). We conclude that, whereas RbAp46/48^{LIN-53} depletion prevents proper CENP-A^{HCP-3} deposition, M18BP1^{KNL-2} and HEC1^{NDC-80} are able to localize to centromeres and assemble kinetochore. Despite the fact that the amounts of kinetochore proteins detected were unchanged in RbAp46/48^{LIN-53} depletion, the chromosome missegregation phenotype (Figures 1E and 1F) indicated that the kinetochore function as a whole is perturbed.

RbAp46/48^{LIN-53} Does Not Affect Global Histone Acetylation

Whereas RbAp46/48^{Mis16} in *S. pombe* maintained histones at the centromeric region in a hypoacetylated state, human RbAp46/48 was suggested to induce histone acetylation during centromere licensing (Hayashi et al., 2004; Fujita et al., 2007). Despite the apparently contradictory results, there is a link between the centromeric function of RbAp46/48 and acetylation regulation in these two models. To determine whether

Figure 2. RbAp46/48^{LIN-53} Localization Is CENP-A^{HCP-3} and M18BP1^{KNL-2} Dependent, and RbAp46/48^{LIN-53} Is Not Required for Kinetochore Protein Recruitment

(A) Representative images of RbAp46/48^{LIN-53} cellular localization in different cell-cycle stages by immunofluorescence. The scale bar represents 5 μm.

(B) RbAp46/48^{LIN-53} interphase and metaphase localization in wild-type, RbAp46/48^{LIN-53}, CENP-A^{HCP-3}, and M18BP1^{KNL-2} RNAi-treated embryos by immunofluorescence. The wild-type images are the same as those in (A). The scale bar represents 5 μm. Quantification of normalized RbAp46/48^{LIN-53} signal intensity in RbAp46/48^{LIN-53}, CENP-A^{HCP-3}, and M18BP1^{KNL-2} RNAi relative to wild-type is shown. The error bars are as in Figure 1B.

(C) GFP::M18BP1^{KNL-2} localization on mitotic chromosomes in one-cell embryos following mock treatment, M18BP1^{KNL-2}, and RbAp46/48^{LIN-53} RNAi. M18BP1^{KNL-2} RNAi served as a positive control. The scale bar represents 10 μm. Quantification of chromosomal GFP::M18BP1^{KNL-2} signal intensity in M18BP1^{KNL-2} and RbAp46/48^{LIN-53} RNAi relative to mock treatment is shown. The error bars are as in Figure 1B.

(D) Immunofluorescence staining of outer kinetochore protein HEC1^{NDC-80} in metaphase in wild-type and RbAp46/48^{LIN-53} RNAi-treated embryos. The scale bar represents 5 μm. Quantification of normalized HEC1^{NDC-80} signal intensity in RbAp46/48^{LIN-53} RNAi relative to wild-type is shown. The error bars are as in Figure 1B.

See also Figure S2.

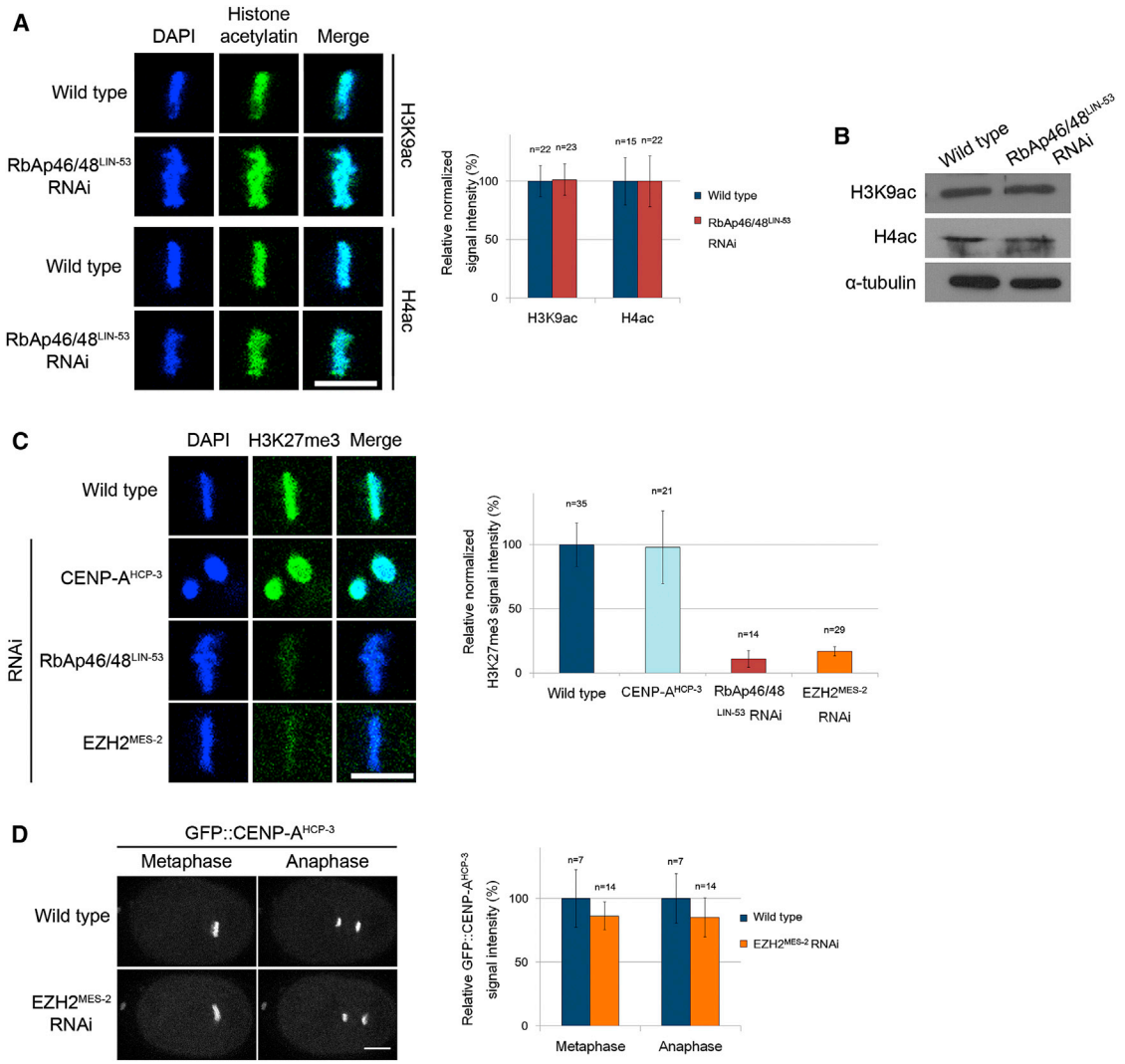

Figure 3. RbAp46/48^{LIN-53} Does Not Regulate CENP-A^{HCP-3} Recruitment through Histone Acetylation or H3K27 Trimethylation

(A) Immunofluorescence staining of H3K9ac and H4K5/8/12/16ac (H4ac) on metaphase chromosomes in wild-type and RbAp46/48^{LIN-53} RNAi-treated embryos. The scale bar represents 5 μm. Quantification of normalized H3K9ac and H4ac signal intensities in RbAp46/48^{LIN-53} RNAi relative to wild-type is shown. The error bars are as in Figure 1B.

(B) Western blot of H3K9ac and H4ac protein levels in wild-type and RbAp46/48^{LIN-53}-depleted whole worms. α-tubulin was used as a loading control.

(C) Immunofluorescence staining of H3K27me3 on metaphase chromosomes in wild-type, CENP-A^{HCP-3}, RbAp46/48^{LIN-53}, and EZH2^{MES-2} RNAi-treated embryos. The scale bar represents 5 μm. Quantification of normalized H3K27me3 signal intensities in CENP-A^{HCP-3}, RbAp46/48^{LIN-53}, and EZH2^{MES-2} RNAi relative to wild-type is shown. The error bars are as in Figure 1B.

(D) GFP::CENP-A^{HCP-3} localization on mitotic chromosomes in wild-type and EZH2^{MES-2} RNAi-treated one-cell embryos by live imaging. The scale bar represents 10 μm. Quantification of chromosomal GFP::CENP-A^{HCP-3} signal intensity in EZH2^{MES-2} RNAi relative to wild-type is shown. The error bars are as in Figure 1B. See also Figure S3.

RbAp46/48^{LIN-53} RNAi affects centromeric or global histone acetylation, we performed immunofluorescence on metaphase chromosomes. In wild-type, the poleward-facing holocentromeric region was not hypoacetylated (Figures 3A and S3), consistent with the lack of negative correlation between CENP-A^{HCP-3} and H3/H4 acetylation from chromatin immunoprecipitation followed by DNA microarray (ChIP-chip) analysis in *C. elegans* (Liu et al., 2011; Gassmann et al., 2012). Although RbAp46/48^{LIN-53} is a component of histone acetyltransferase complex (HAT1), nucleosome remodeling and histone deacetylation complex (NuRD), and Sin3 histone deacetylation complex (Ai and Parthun, 2004; Hassig et al., 1997; Parthun et al., 1996; Xue et al., 1998), global H3K9 and H4 acetylation (H3K9ac and H4K5/8/12/16ac) levels after RbAp46/48^{LIN-53} RNAi were comparable to wild-type by immunofluorescence (Figure 3A) and western blot (Figure 3B). These results suggest that RbAp46/48^{LIN-53} does not regulate CENP-A^{HCP-3} centromeric localization via histone acetylation in *C. elegans*.

A

RbAp46/48^{LIN-53}-containing complex	Functions	Core component	References
Polycomb repressor complex 2 (PRC2)	H3K27 methylation and gene silencing	EZH2^{MES-2}	Kuzmichev et al., 2002; Muller et al., 2002
Histone acetyltransferase complex (HAT1)	Histone acetylation	HAT-1$^{TAG-235}$	Ai and Parthun, 2004; Parthun et al., 1996
Nucleosome remodeling and histone deacetylation complex (NuRD)	Nucleosome remodeling and histone deacetylation	CHD4$^{LET-418}$	Xue et al., 1998
Nucleosome remodeling factor complex (NuRF)	Nucleosome remodeling	NURF301^{NURF-1}	Martinez-Balbas et al., 1998
Chromatin assembly factor-1 complex (CAF-1)	Chromatin assembly	CHAF-1	Verreault et al., 1996
Histone deacetylation complex (Sin3)	Histone deacetylation	SIN-3	Hassig et al., 1997
Dp, Rb, MuvB complex (DRM)	Transcriptional repression	LIN-54	Harrison et al., 2006

B

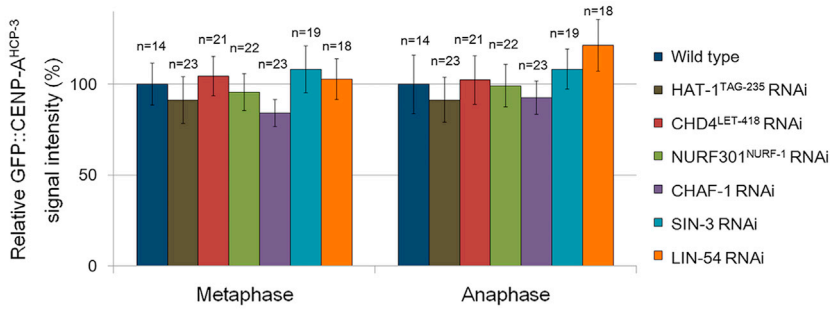

C

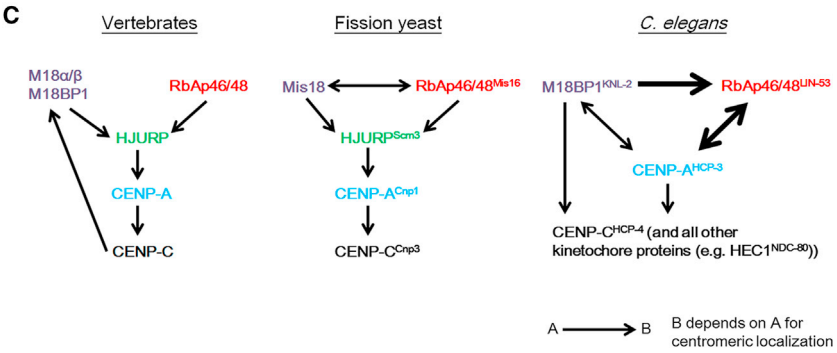

Figure 4. RbAp46/48^{LIN-53} Does Not Regulate CENP-A^{HCP-3} Recruitment through Its Known Chromatin-Modifying Complexes

(A) Table of RbAp46/48^{LIN-53}-containing complexes, their functions, and their core components.

(B) Quantification of GFP::CENP-A^{HCP-3} signal intensity on mitotic chromosomes upon depletion of different complexes' core component relative to wild-type. The error bars are as in Figure 1B.

(C) A schematic diagram of the centromeric localization dependency in vertebrates, fission yeast, and *C. elegans*. Homologs are represented by the same color. Bold arrows indicate the findings from this study.

See also Figure S4.

RbAp46/48^{LIN-53} Does Not Regulate CENP-A^{HCP-3} Recruitment through the H3K27-Methylating PRC2 Complex or Other Known Chromatin-Modifying Complexes

In *C. elegans*, RbAp46/48^{LIN-53} is a component of various chromatin-modifying complexes involved in nucleosome assembly, histone modifications, and gene regulation (Figure 4A). One of the RbAp46/48^{LIN-53}-containing complexes, polycomb repressor complex 2 (PRC2), has a role in generating the transcriptional repression mark, trimethylated H3 at K27 (H3K27me3), for gene silencing (Bender et al., 2004). This mark positively correlated (correlation index = 0.64) with CENP-A^{HCP-3} based on ChIP-chip analysis in *C. elegans* (Gassmann et al., 2012), but whether a causal relationship exists between H3K27me3 and CENP-A^{HCP-3} localization is unknown. However, when we analyzed the H3K27me3 pattern on wild-type metaphase chromosomes by immunofluorescence, we did not observe an enrichment of this modification at centromeres at this resolution (Figure 3C). Depletion of CENP-A^{HCP-3} did not affect the level of chromosomal H3K27me3, but RbAp46/48^{LIN-53} depletion reduced H3K27me3 level on metaphase chromosomes to 11% compared to wild-type (Figure 3C). To test whether RbAp46/48^{LIN-53} depletion affects CENP-A^{HCP-3} localization through modulating H3K27me3 level, we depleted histone methyltransferase EZH2^{MES-2} in PRC2 complex, which reduced chromosomal H3K27me3 level to 17% of wild-type (Figure 3C). However, EZH2^{MES-2} depletion did not significantly reduce centromeric GFP::CENP-A^{HCP-3} level (Figure 3D). This suggests that RbAp46/48^{LIN-53} does not recruit CENP-A^{HCP-3} to the centromere through PRC2 complex. We also systematically depleted the core enzymatic component or the largest subunit of the other six RbAp46/48^{LIN-53}-containing complexes (Figure 4A). None of these perturbations led to a decrease in centromeric GFP::CENP-A^{HCP-3} level (Figures 4B and S4). These results suggest that RbAp46/48^{LIN-53}'s role in centromeric CENP-A^{HCP-3} deposition may be independent of its roles as part of these known chromatin-modifying complexes.

DISCUSSION

Here, we establish a role for RbAp46/48^{LIN-53} in CENP-A^{HCP-3} centromeric localization and chromosome segregation, consistent with its homolog's function in flies, humans, and fission yeast (Figure 4C; Furuyama et al., 2006; Hayashi et al., 2004). The localization pattern of RbAp46/48^{LIN-53} provides clues to

the deposition timing of CENP-A^{HCP-3}. In humans, RbAp46/48 dissociates from chromatin upon mitotic entry and reassociates again in late mitosis, which is coincident with Mis18 complex centromeric localization time, and slightly before CENP-A deposition (Fujita et al., 2007; Hayashi et al., 2004; Jansen et al., 2007). In *C. elegans*, we found that RbAp46/48^{LIN-53} and CENP-A^{HCP-3} colocalize at the centromere in metaphase. Because RbAp46/48^{LIN-53} disappears from the centromere in anaphase, RbAp46/48^{LIN-53}-mediated CENP-A^{HCP-3} deposition is likely to occur before anaphase.

Surprisingly, RbAp46/48^{LIN-53} depletion affects CENP-A^{HCP-3} recruitment without perturbing kinetochore assembly. We speculate that the ~5% of residual CENP-A^{HCP-3} level in RbAp46/48^{LIN-53} depletion is sufficient to recruit M18BP1^{KNL-2} and other kinetochore proteins. This is consistent with data in human cells, where 1% of centromeric CENP-A is sufficient to recruit kinetochore proteins and support partial centromere function (Fachinetti et al., 2013). Alternatively, there may be a CENP-A^{HCP-3}-independent pathway for M18BP1^{KNL-2} centromere assembly that remains to be identified. Interestingly, Maddox et al. (2007) showed that M18BP1^{KNL-2} depletion resulted in a similar level of residual CENP-A^{HCP-3} on chromosomes as RbAp46/48^{LIN-53} depletion, yet no other kinetochore proteins could be recruited to the centromere. These results suggest that M18BP1^{KNL-2}, but not RbAp46/48^{LIN-53}, is critical for building the kinetochore in *C. elegans*. Our localization dependency results also put licensing factor M18BP1^{KNL-2} upstream of RbAp46/48^{LIN-53} in the centromeric chromatin assembly hierarchy (Figure 4C). Despite the fact that RbAp46/48^{LIN-53} is not required for kinetochore assembly, its role in ensuring full CENP-A^{HCP-3} recruitment is crucial for faithful chromosome segregation. These results suggest that kinetochores containing a low level of CENP-A^{HCP-3} are not fully functional.

Mechanistically, we show that RbAp46/48^{LIN-53} does not regulate centromere function via histone acetylation, in contrast to its human and fission yeast homologs (Fujita et al., 2007; Hayashi et al., 2004), nor through H3K27 trimethylation. This may reflect the fact that holocentromeres are more plastic than monocentromeres because holocentromeres are not flanked by heterochromatin as in most monocentromeres, and no histone modification so far is known to affect holocentromere function. We also found that RbAp46/48^{LIN-53} does not affect CENP-A^{HCP-3} through its known chromatin-modifying complexes, though we cannot exclude the possibility that RbAp46/48^{LIN-53} might participate in novel complexes. As no HJURP^{Scm3} homolog has been identified in *C. elegans*, RbAp46/48^{LIN-53} may serve this escort function. Whether RbAp46/48^{LIN-53} can assemble CENP-A^{CID}-H4 dimers in vitro like its *Drosophila* homolog (Furuyama et al., 2006) remains to be determined. In agreement with a chaperone role for CENP-A^{HCP-3}, we show that RbAp46/48^{LIN-53} is required for CENP-A^{HCP-3} protein stability, but not mRNA stability, similar to the results in human cells (Hayashi et al., 2004). Indeed, RbAp46/48^{LIN-53} depletion has a more-pronounced effect on the protein level of CENP-A^{HCP-3} than histone H3.

In conclusion, we found that the conserved histone chaperone RbAp46/48^{LIN-53} is required for the recruitment of CENP-A^{HCP-3} to holocentromeres in *C. elegans*, like in vertebrate, fission yeast, and fly centromeres. RbAp46/48^{LIN-53} and M18BP1^{KNL-2} are the only two factors identified to date that are required for CENP-A^{HCP-3} localization in *C. elegans*. We revealed the centromeric localization interdependency between RbAp46/48^{LIN-53} and CENP-A^{HCP-3} (Figure 4C) and the functional relationship between RbAp46/48^{LIN-53} and other centromeric proteins. We propose that the function of RbAp46/48^{LIN-53} at *C. elegans* holocentromeres may not lie in licensing but that instead RbAp46/48^{LIN-53} serves as a chaperone for CENP-A^{HCP-3}, similar to the role of HJURP^{Scm3} in other organisms. This study opens avenues for studying the temporal and spatial regulation of CENP-A^{HCP-3} deposition at holocentromeres and offers new perspectives for a comprehensive comparison of centromere assembly between monocentromeres and holocentromeres.

EXPERIMENTAL PROCEDURES

Co-immunoprecipitation

About 110 μl of N2 embryonic extract (2.14 mg/ml) was incubated with 1 μg of anti-CENP-A^{HCP-3} antibody (OD80; a gift from Arshad Desai), anti-RbAp46/48^{LIN-53} antibody (Novus SDQ2370), or rabbit IgG (Abcam) at 4°C overnight. 0.9 mg (30 μl) of Dynabeads protein A (Invitrogen) was then added to pull down the antibody-antigen complex. After washing three times by 1× IP buffer (50 mM NaCl; Invitrogen), 45 μl elution buffer was used to elute target antigen complex. One-third of the eluate from each IP sample, and 18% of input, was blotted by anti-CENP-A^{HCP-3} antibody (1:2,000; Novus 29540002 SDQ0804) as primary antibody and goat-anti-rabbit IgG horseradish peroxidase (HRP) (1:100,000; Abcam ab97051) as secondary antibody or anti-RbAp46/48^{LIN-53} antibody (1:2,000; Novus 38710002 SDQ2370) as primary antibody and protein A HRP (1:150,000; Abcam ab7456) as secondary antibody.

dsRNA Production

Eight hundred to one thousand base pairs coding region of targeted genes was amplified from N2 *C. elegans* cDNA using primers with 5′ flanking T3 (forward) and T7 (reverse) promoter sequences (listed in Table S2). Purified PCR products were subjected to in vitro transcription (MEGAscript Transcription Kit; Life Technologies). Reaction products were digested with TURBO DNase at 37°C for 15 min and purified (MEGAclear Kit; Life Technologies). Eluates were incubated at 68°C for 10 min followed by 37°C for 30 min to generate dsRNA. Purified dsRNA was mixed with 10× soaking buffer (109 mM Na_2HPO_4, 55 mM KH_2PO_4, 21 mM NaCl, 47 mM NH_4Cl, and nuclease-free [DEPC-treated] H_2O) to yield a concentration of >1 μg/μl.

RNAi

L4 hermaphrodites were soaked in dsRNA solution containing 3 mM spermidine and 0.05% gelatin at 22°C for 24 hr and recovered at 22°C for 24 hr before analysis. In mock treatment, 10× soaking buffer with spermidine and gelatin were used.

Live-Cell Imaging

Preparation and mounting of OD421, AV221, and OD85 (Table S3) embryos were performed as described (Powers, 2010). All images were acquired using Perkin-Elmer UltraView ERS spinning disk system (PerkinElmer) with an inverted Axio Observer (Carl Zeiss) at 22°C, a 63× 1.4 NA oil objective, and an Evolve 512 EMCCD camera. Embryos were captured in stacks of 12 sections along z axis at 1-μm intervals. Images were taken at 25 s intervals with 200 ms and 400 ms exposures at the 488-nm (30%) and 543-nm (45%) channels, respectively.

Western Blotting

Equal number of wild-type and RNAi-treated adult worms were lysed in 75 μl M9/0.1% Triton X-100 (3 g KH_2PO_4, 6 g Na_2HPO_4, 5 g NaCl, 1 ml 1 M $MgSO_4$, 1 ml Triton X-100, and H_2O to 1l) and 25 μl 4× sample buffer (8% SDS,

0.04% bromophenol blue, 240 mM Tris/HCl [pH 6.8], 40% glycerol, and 5% β-mercaptoethanol) using water bath sonication at 4°C for 20 min. Ten worms were loaded in each lane for SDS-PAGE. Proteins were transferred to nitrocellulose membranes and probed using antibodies against α-tubulin (1:8,000; Abcam ab7291 DM1A), RbAp46/48^{LIN-53} (1:400; abm SAB494-1), CENP-A^{HCP-3} (1:1,000; Novus 29540002 SDQ0806 or SDQ0804), mCherry (1:500; Abcam ab167453), H3K9ac (1:1,000; Millipore ABE18), H4ac (1:1,000; Millipore 06-598; recognizing acetylated lysines 5, 8, 12, and 16 of Tetrahymena histone H4), H3 (1:5,000; Abcam ab1791), H4 (1:1,000; Abcam ab10158), or mCherry (1:500; Abcam ab167453) at 4°C overnight. After washes with TBST, immunoblots were subjected to HRP-conjugated antibodies incubation (Abcam ab97051 or ab97023) at room temperature for 1 hr. Blot signals were detected using Amersham ECL Select western blotting detection reagent (GE Healthcare Life Sciences).

Immunofluorescence

After dissection of N2 and AV221 (Table S3) gravid hermaphrodites, embryos were freeze-cracked in liquid nitrogen, fixed in methanol at −20°C for 30 min, rehydrated in PBS for 5 min, and blocked in AbDil (4% BSA and 0.1% Triton X-100 in PBS) at room temperature for 20 min. Incubation of primary antibody against RbAp48^{p55} (1:100; Abcam ab53616), CENP-A^{HCP-3} (1:2,000; Novus 29540002 SDQ0804), M18BP1^{KNL-2} (1:1,000; SDQ0803, a gift from the Desai lab), HEC1^{NDC-80} (1:1,000; OD32, a gift from the Desai lab), lacI (1:500; Millipore 05-503), H3K9ac (1:1,000; Millipore ABE18), H4ac (1:500; Millipore 06-598), or H3K27me3 (1:500; Millipore 07-449) was done at 4°C overnight. Slides were washed with PBST before FITC-conjugated secondary antibody (1:200; Jackson ImmunoResearch Laboratories) incubation at room temperature for 1 hr. Mounting was done using ProLong gold antifade reagent with DAPI (Life Technologies). Images were acquired from Zeiss LSM 710 upright confocal microscope with a 63× 1.4 NA oil objective and PMT detectors. Embryos were captured as z stacks with a z step size at 0.5 μm and 1.58 μs of pixel dwell time.

Image Quantification

All images were analyzed using ImageJ 1.45 software. For live-cell imaging, z stack images were subjected to maximum projection before quantification. Immunofluorescence images were quantified using a single z section. A fixed area capturing metaphase or anaphase chromosomes (A) and an area enclosing area A within the embryo (B) were selected and quantified in each sample. For each channel, integrated signal intensities in A and B were measured as A^I and B^I, respectively. Average background intensity (Y) was estimated as $(B^I–A^I)/(B–A)$. Average signal intensity was estimated as $(A^I–Y \times A)/A$. For live-cell imaging, average signal intensity of each channel was compared to mock treatment. For immunofluorescence, average signal intensity of the 488-nm channel was normalized with that of DAPI.

RT-PCR

An equal number of wild-type and RNAi-treated adult worms were subjected to RNA extraction using standard TRIzol (Life Technologies) method. Reverse transcription was done using iScript cDNA Synthesis Kit (Bio-Rad).

SUPPLEMENTAL INFORMATION

Supplemental Information includes Supplemental Experimental Procedures, four figures, three tables, and four movies and can be found with this article online at http://dx.doi.org/10.1016/j.celrep.2016.01.065.

AUTHOR CONTRIBUTIONS

Conceptualization, K.W.Y.Y.; Methodology, B.C.H.L., Z.L., and K.W.Y.Y.; Investigation, B.C.H.L. and Z.L.; Validation, B.C.H.L. and Z.L.; Visualization, B.C.H.L., Z.L., and K.W.Y.Y., Writing – Original Draft, B.C.H.L. and K.W.Y.Y.; Writing – Review & Editing, B.C.H.L., Z.L., and K.W.Y.Y.; Supervision, K.W.Y.Y.; Project Administration, K.W.Y.Y.; Funding Acquisition, K.W.Y.Y.

ACKNOWLEDGMENTS

We thank Arshad Desai for strains and antibodies, Robert Horvitz and Caenorhabditis Genetics Center for strains, and Sherry Niessen for assistance in mass spectrometry analysis. We thank Reto Gassmann, Dhanya Cheerambathur, Deigo Folco, Valeria Viscardi, Arshad Desai, and Alice Wong for critical reading of the manuscript and comments. We are grateful to the University of Hong Kong School of Biological Sciences Central Facilities and Li Ka Shing Faculty of Medicine Faculty Core Facility for the microscopy facility. This project is supported by the HK Research Grant Council (RGC) General Research Grant (GRF) (project number: 785313) and the HKU Seed Fund for Basic Research (project code: 201112159003).

Received: August 10, 2015
Revised: December 1, 2015
Accepted: January 21, 2016
Published: February 18, 2016

REFERENCES

Ai, X., and Parthun, M.R. (2004). The nuclear Hat1p/Hat2p complex: a molecular link between type B histone acetyltransferases and chromatin assembly. Mol. Cell *14*, 195–205.

Barnhart, M.C., Kuich, P.H., Stellfox, M.E., Ward, J.A., Bassett, E.A., Black, B.E., and Foltz, D.R. (2011). HJURP is a CENP-A chromatin assembly factor sufficient to form a functional de novo kinetochore. J. Cell Biol. *194*, 229–243.

Bender, L.B., Cao, R., Zhang, Y., and Strome, S. (2004). The MES-2/MES-3/MES-6 complex and regulation of histone H3 methylation in C. elegans. Curr. Biol. *14*, 1639–1643.

Bernad, R., Sánchez, P., Rivera, T., Rodríguez-Corsino, M., Boyarchuk, E., Vassias, I., Ray-Gallet, D., Arnaoutov, A., Dasso, M., Almouzni, G., and Losada, A. (2011). Xenopus HJURP and condensin II are required for CENP-A assembly. J. Cell Biol. *192*, 569–582.

Camahort, R., Li, B., Florens, L., Swanson, S.K., Washburn, M.P., and Gerton, J.L. (2007). Scm3 is essential to recruit the histone h3 variant cse4 to centromeres and to maintain a functional kinetochore. Mol. Cell *26*, 853–865.

Dambacher, S., Deng, W., Hahn, M., Sadic, D., Fröhlich, J., Nuber, A., Hoischen, C., Diekmann, S., Leonhardt, H., and Schotta, G. (2012). CENP-C facilitates the recruitment of M18BP1 to centromeric chromatin. Nucleus *3*, 101–110.

Dunleavy, E.M., Roche, D., Tagami, H., Lacoste, N., Ray-Gallet, D., Nakamura, Y., Daigo, Y., Nakatani, Y., and Almouzni-Pettinotti, G. (2009). HJURP is a cell-cycle-dependent maintenance and deposition factor of CENP-A at centromeres. Cell *137*, 485–497.

Fachinetti, D., Folco, H.D., Nechemia-Arbely, Y., Valente, L.P., Nguyen, K., Wong, A.J., Zhu, Q., Holland, A.J., Desai, A., Jansen, L.E., and Cleveland, D.W. (2013). A two-step mechanism for epigenetic specification of centromere identity and function. Nat. Cell Biol. *15*, 1056–1066.

Foltz, D.R., Jansen, L.E., Bailey, A.O., Yates, J.R., 3rd, Bassett, E.A., Wood, S., Black, B.E., and Cleveland, D.W. (2009). Centromere-specific assembly of CENP-a nucleosomes is mediated by HJURP. Cell *137*, 472–484.

Fujita, Y., Hayashi, T., Kiyomitsu, T., Toyoda, Y., Kokubu, A., Obuse, C., and Yanagida, M. (2007). Priming of centromere for CENP-A recruitment by human hMis18alpha, hMis18beta, and M18BP1. Dev. Cell *12*, 17–30.

Furuyama, T., Dalal, Y., and Henikoff, S. (2006). Chaperone-mediated assembly of centromeric chromatin in vitro. Proc. Natl. Acad. Sci. USA *103*, 6172–6177.

Gassmann, R., Rechtsteiner, A., Yuen, K.W., Muroyama, A., Egelhofer, T., Gaydos, L., Barron, F., Maddox, P., Essex, A., Monen, J., et al. (2012). An inverse relationship to germline transcription defines centromeric chromatin in C. elegans. Nature *484*, 534–537.

Harrison, M.M., Ceol, C.J., Lu, X., and Horvitz, H.R. (2006). Some C. elegans class B synthetic multivulva proteins encode a conserved LIN-35

Rb-containing complex distinct from a NuRD-like complex. Proc. Natl. Acad. Sci. USA *103*, 16782–16787.

Hassig, C.A., Fleischer, T.C., Billin, A.N., Schreiber, S.L., and Ayer, D.E. (1997). Histone deacetylase activity is required for full transcriptional repression by mSin3A. Cell *89*, 341–347.

Hayashi, T., Fujita, Y., Iwasaki, O., Adachi, Y., Takahashi, K., and Yanagida, M. (2004). Mis16 and Mis18 are required for CENP-A loading and histone deacetylation at centromeres. Cell *118*, 715–729.

Jansen, L.E., Black, B.E., Foltz, D.R., and Cleveland, D.W. (2007). Propagation of centromeric chromatin requires exit from mitosis. J. Cell Biol. *176*, 795–805.

Kitagawa, R. (2009). Key players in chromosome segregation in Caenorhabditis elegans. Front. Biosci. (Landmark) *14*, 1529–1557.

Kuzmichev, A., Nishioka, K., Erdjument-Bromage, H., Tempst, P., and Reinberg, D. (2002). Histone methyltransferase activity associated with a human multiprotein complex containing the Enhancer of Zeste protein. Genes Dev. *16*, 2893–2905.

Liu, T., Rechtsteiner, A., Egelhofer, T.A., Vielle, A., Latorre, I., Cheung, M.S., Ercan, S., Ikegami, K., Jensen, M., Kolasinska-Zwierz, P., et al. (2011). Broad chromosomal domains of histone modification patterns in C. elegans. Genome Res. *21*, 227–236.

Lu, X., and Horvitz, H.R. (1998). lin-35 and lin-53, two genes that antagonize a C. elegans Ras pathway, encode proteins similar to Rb and its binding protein RbAp48. Cell *95*, 981–991.

Maddox, P.S., Hyndman, F., Monen, J., Oegema, K., and Desai, A. (2007). Functional genomics identifies a Myb domain-containing protein family required for assembly of CENP-A chromatin. J. Cell Biol. *176*, 757–763.

Martínez-Balbás, M.A., Tsukiyama, T., Gdula, D., and Wu, C. (1998). Drosophila NURF-55, a WD repeat protein involved in histone metabolism. Proc. Natl. Acad. Sci. USA *95*, 132–137.

McKinley, K.L., and Cheeseman, I.M. (2014). Polo-like kinase 1 licenses CENP-A deposition at centromeres. Cell *158*, 397–411.

Mizuguchi, G., Xiao, H., Wisniewski, J., Smith, M.M., and Wu, C. (2007). Nonhistone Scm3 and histones CenH3-H4 assemble the core of centromere-specific nucleosomes. Cell *129*, 1153–1164.

Moree, B., Meyer, C.B., Fuller, C.J., and Straight, A.F. (2011). CENP-C recruits M18BP1 to centromeres to promote CENP-A chromatin assembly. J. Cell Biol. *194*, 855–871.

Müller, J., Hart, C.M., Francis, N.J., Vargas, M.L., Sengupta, A., Wild, B., Miller, E.L., O'Connor, M.B., Kingston, R.E., and Simon, J.A. (2002). Histone methyltransferase activity of a Drosophila Polycomb group repressor complex. Cell *111*, 197–208.

Parthun, M.R., Widom, J., and Gottschling, D.E. (1996). The major cytoplasmic histone acetyltransferase in yeast: links to chromatin replication and histone metabolism. Cell *87*, 85–94.

Pearson, C.G., Yeh, E., Gardner, M., Odde, D., Salmon, E.D., and Bloom, K. (2004). Stable kinetochore-microtubule attachment constrains centromere positioning in metaphase. Curr. Biol. *14*, 1962–1967.

Pidoux, A.L., Choi, E.S., Abbott, J.K., Liu, X., Kagansky, A., Castillo, A.G., Hamilton, G.L., Richardson, W., Rappsilber, J., He, X., and Allshire, R.C. (2009). Fission yeast Scm3: A CENP-A receptor required for integrity of subkinetochore chromatin. Mol. Cell *33*, 299–311.

Powers, J.A. (2010). Live-cell imaging of mitosis in Caenorhabditis elegans embryos. Methods *51*, 197–205.

Shelby, R.D., Monier, K., and Sullivan, K.F. (2000). Chromatin assembly at kinetochores is uncoupled from DNA replication. J. Cell Biol. *151*, 1113–1118.

Silva, M.C., Bodor, D.L., Stellfox, M.E., Martins, N.M., Hochegger, H., Foltz, D.R., and Jansen, L.E. (2012). Cdk activity couples epigenetic centromere inheritance to cell cycle progression. Dev. Cell *22*, 52–63.

Takayama, Y., Sato, H., Saitoh, S., Ogiyama, Y., Masuda, F., and Takahashi, K. (2008). Biphasic incorporation of centromeric histone CENP-A in fission yeast. Mol. Biol. Cell *19*, 682–690.

Tursun, B., Patel, T., Kratsios, P., and Hobert, O. (2011). Direct conversion of C. elegans germ cells into specific neuron types. Science *331*, 304–308.

Verreault, A., Kaufman, P.D., Kobayashi, R., and Stillman, B. (1996). Nucleosome assembly by a complex of CAF-1 and acetylated histones H3/H4. Cell *87*, 95–104.

Verreault, A., Kaufman, P.D., Kobayashi, R., and Stillman, B. (1998). Nucleosomal DNA regulates the core-histone-binding subunit of the human Hat1 acetyltransferase. Curr. Biol. *8*, 96–108.

Williams, J.S., Hayashi, T., Yanagida, M., and Russell, P. (2009). Fission yeast Scm3 mediates stable assembly of Cnp1/CENP-A into centromeric chromatin. Mol. Cell *33*, 287–298.

Xue, Y., Wong, J., Moreno, G.T., Young, M.K., Côté, J., and Wang, W. (1998). NURD, a novel complex with both ATP-dependent chromatin-remodeling and histone deacetylase activities. Mol. Cell *2*, 851–861.

Cell Reports, Volume *14*

Supplemental Information

RbAp46/48^{LIN-53} Is Required for Holocentromere Assembly in *Caenorhabditis elegans*

Bernard Chi Hang Lee, Zhongyang Lin, and Karen Wing Yee Yuen

S1A

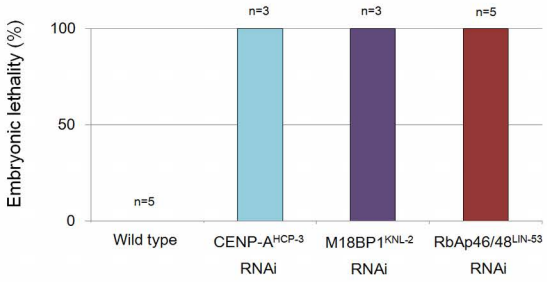

S1B

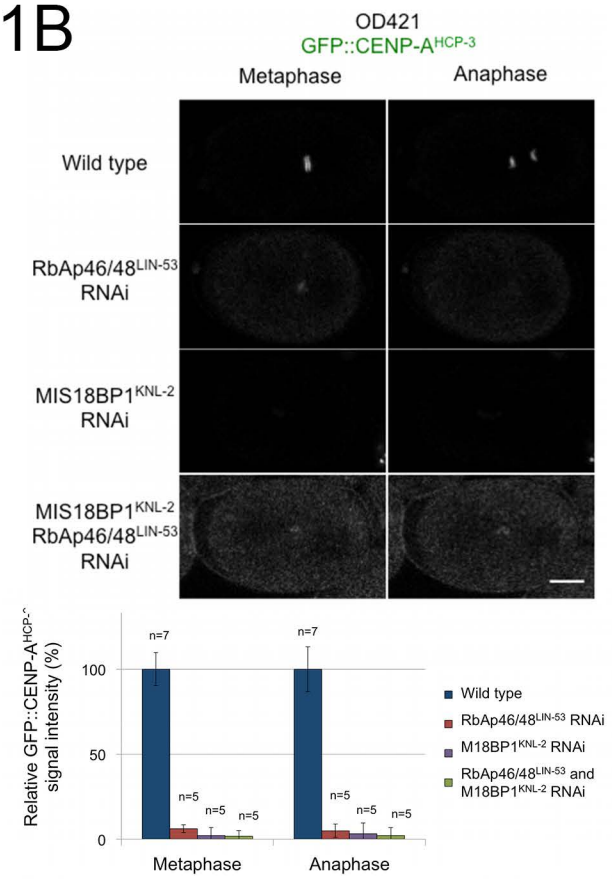

S1C

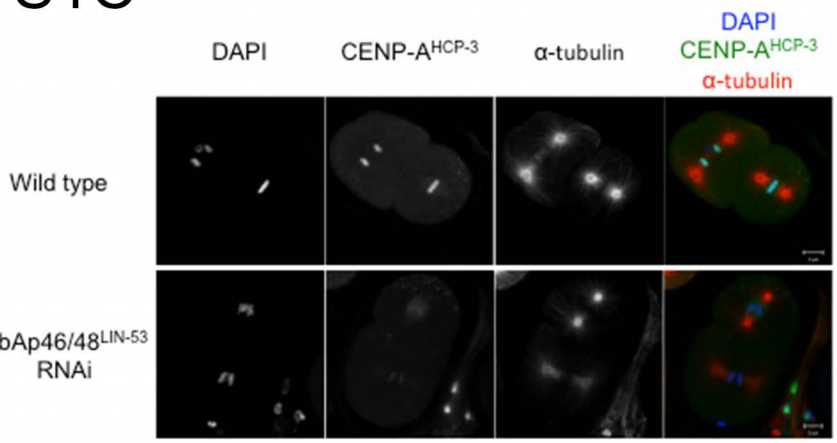

S1D

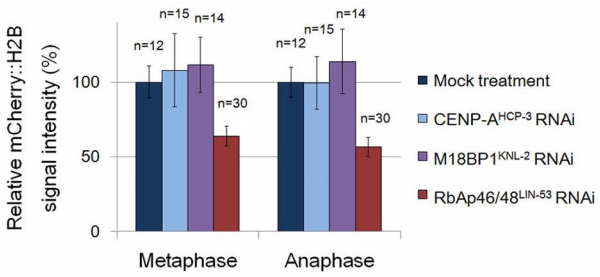

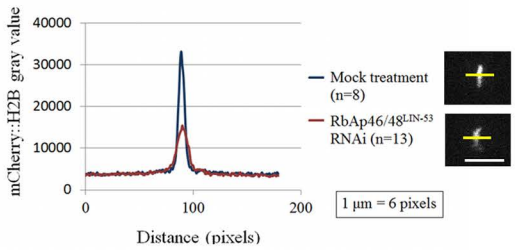

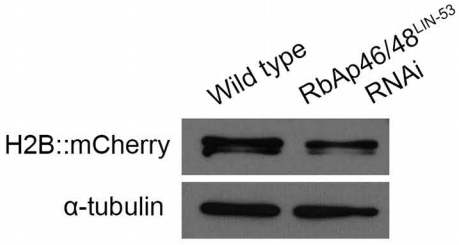

S1E

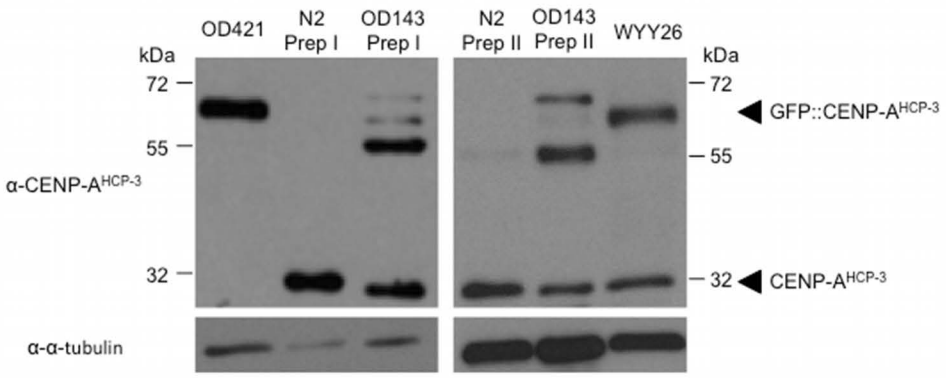

S1F

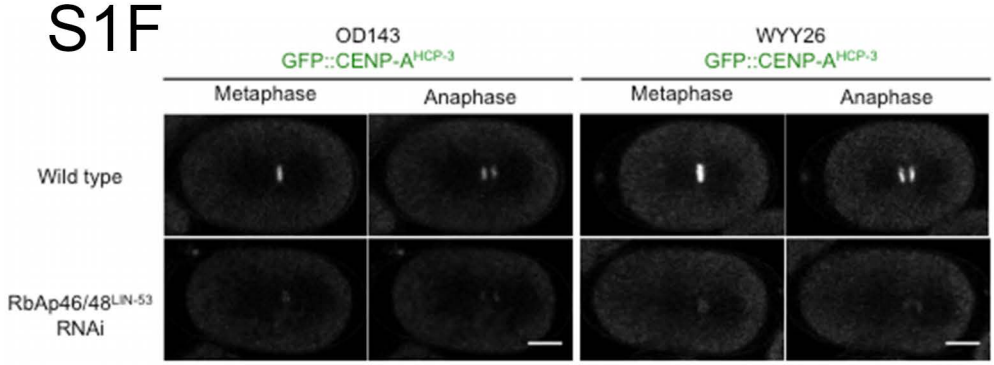

S1G

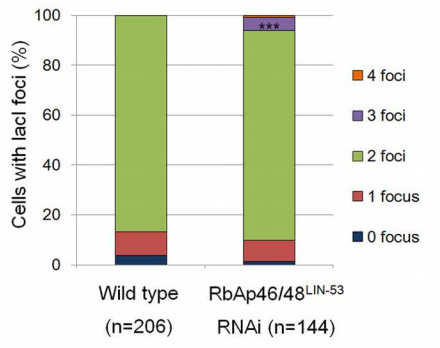

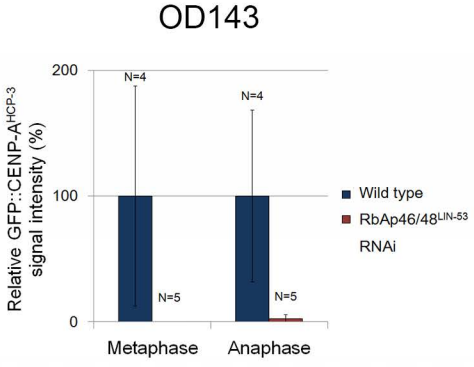

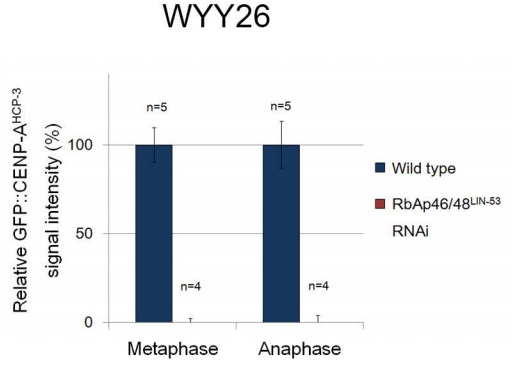

Fig. S1 Validation of the efficiency of RNAi, and validation of the endogenous localization of GFP::CENP-A^{HCP-3}, related to Fig. 1

(A) CENP-A^{HCP-3}, M18BP1^{KNL-2} or RbAp46/48^{LIN-53} RNAi by soaking resulted in 100% embryonic lethality, suggesting the depletions by RNAi were efficient**.** Embryonic lethality was estimated from the average of 3-5 independent RNAi experiments. Error bars as in Fig. 1B.

(B) Representative live-cell images and quantification of GFP::CENP-A^{HCP-3} (in OD421) signal intensity on mitotic chromosomes after RbAp46/48^{LIN-53}, M18BP1^{KNL-2} or RbAp46/48^{LIN-53} M18BP1^{KNL-2} double RNAi by injection, relative to wild type. The delocalization of GFP::CENP-A^{HCP-3} in the double RNAi was comparable to that in RbAp46/48^{LIN-53} or M18BP1^{KNL-2} single RNAi by injection, suggesting there is no synergistic effect. RbAp46/48^{LIN-53} and M18BP1^{KNL-2} function in the same CENP-A^{HCP-3} assembly pathway. The delocalization of GFP::CENP-A^{HCP-3} in RbAp46/48^{LIN-53} or M18BP1^{KNL-2} single RNAi by injection was slightly more potent than that by soaking RNAi (Fig. 1A), but are fairly consistent. Scale bar: 10 μm. Error bars as in Fig. 1B.

(C) Representative immunofluorescence images of CENP-A^{HCP-3} (Novus 29540002 SDQ0804) in wild type embryos and in RbAp46/48^{lin-53} injection RNAi. Scale bar: 5 μm. Chromosomal and kinetochore CENP-A^{HCP-3} was significantly reduced in RbAp46/48^{lin-53} injection RNAi, consistent with live imaging results of GFP::CENP-A^{HCP-3} in Fig. 1A.

(D) Quantification of chromosomal mCherry::H2B in CENP-A^{HCP-3}, M18BP1^{KNL-2} or RbAp46/48^{LIN-53} soaking RNAi, corresponding to Fig. 1B. Chromosomal mCherry::H2B was reduced to ~60% of wild type in RbAp46/48^{LIN-53} soaking RNAi. Error bars as in Fig. 1B. However, line scan analysis of the average mCherry::H2B signal across the metaphase plate showed that the width of the metaphase plate was not changed in RbAp46/48^{LIN-53} soaking RNAi. Western blot analysis using anti-mCherry antibody (1:500; abcam® ab167453) showed that the transgene mCherry::H2B protein level was also reduced to ~65% of wild type.

(E) Western blot analysis of CENP-A^{HCP-3} (Novus 29540002 SDQ0804) in N2 wild type, OD143, WYY26 and OD421 (Table S3). The endogenous levels of CENP-A^{HCP-3} in OD143 and WYY26 were comparable to that in N2 wild type. OD143, WYY26 and OD421 showed GFP::CENP-A^{HCP-3} expression. Multiple bands close to the size of GFP::CENP-A^{HCP-3} appear in OD143, possibly due to multiple-copy insertion of different sizes, and unlikely due to protein degradation because different preparations of extracts show similar pattern with no other degradation. Therefore, considering both endogenous CENP-A^{HCP-3} and

transgenic GFP::CENP-A^{HCP-3} together, OD143 and WYY26 have increased total level of CENP-A^{HCP-3}. OD421 only contains GFP::CENP-A^{HCP-3} but not endogenous CENP-A^{HCP-3}.

(F) Representative live-cell images and quantification of GFP::CENP-A^{HCP-3} signal intensity on mitotic chromosomes in CENP-A^{HCP-3}-overexpressed strains (OD143 and WYY26) after RbAp46/48^{LIN-53} injection RNAi, relative to mock treatment. Delocalization of GFP::CENP-A^{HCP-3} was similar to that in Fig. 1B (in OD421), suggesting that overexpression of GFP::CENP-A^{HCP-3} did not rescue CENP-A^{HCP-3} localization defect in RbAp46/48^{LIN-53} depletion. Scale bar: 10 μm. Error bars represent standard deviation of the mean.

(G) Quantification of the percentage of cells with 0 to 4 GFP::lacI foci in wild type and RbAp46/48^{LIN-53} RNAi in 17-32 cell stages. Chi square test was used to test significance. ***, $P < 0.001$. This result is similar to that in 8-16 cell stages in Fig. 1F.

S2A

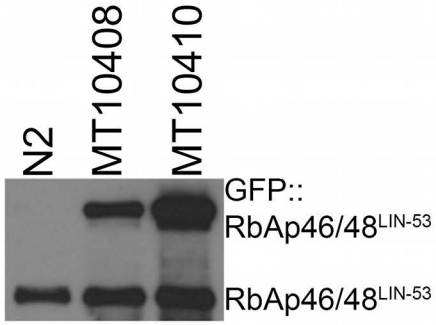

S2B

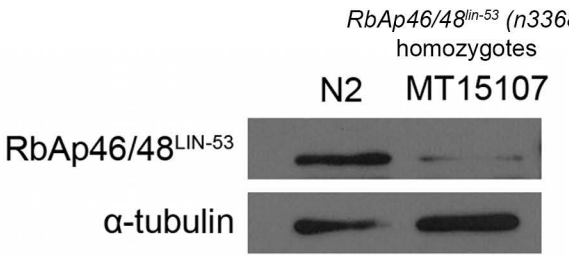

S2C

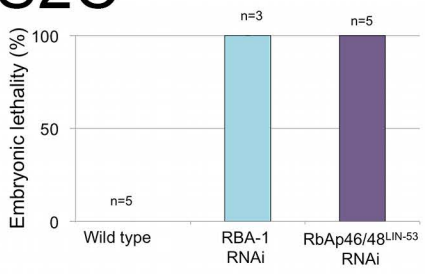

S2D

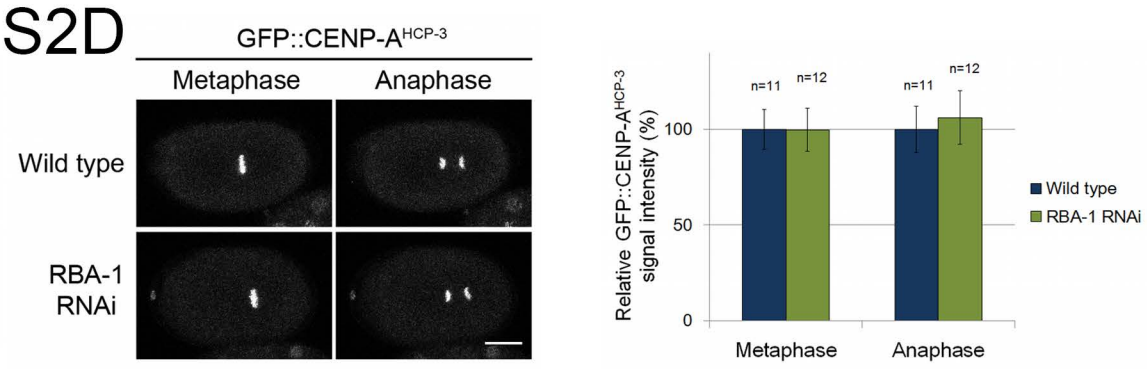

S2E

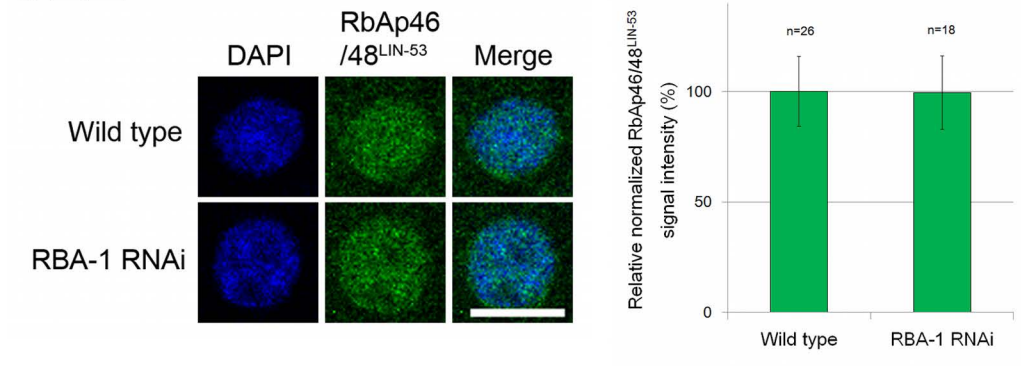

S2F

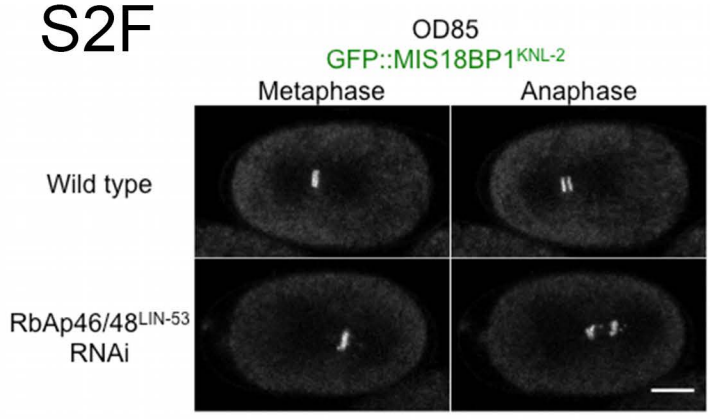

S2G

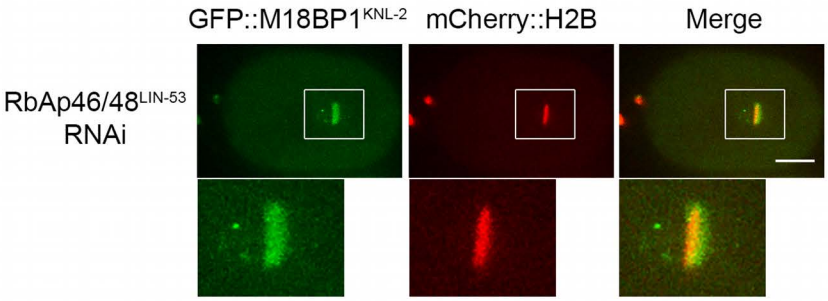

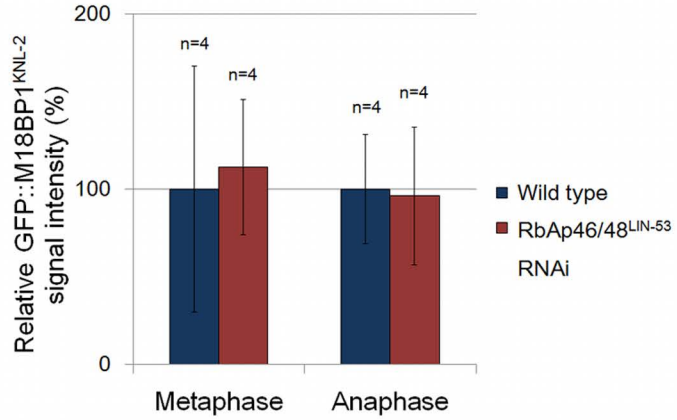

S2H

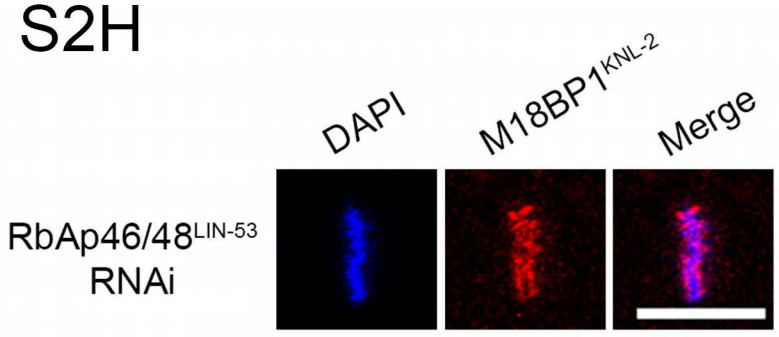

Fig. S2 Validation of RbAp46/48^{LIN-53} RNAi specificity and RbAp46/48^{LIN-53} antibodies specificity, related to Fig. 1 and 2

(A) Western blot analysis of RbAp46/48^{LIN-53} in N2 wild type, GFP::RbAp46/48^{LIN-53} transgenic strains MT10408 and MT10410 (Table S3) using the RbAp46/48^{LIN-53} antibody for co-immunoprecipitation (Fig. 1A; Novus 38710002 SDQ2370). Both endogenous and GFP::RbAp46/48^{lin-53} were detected, indicating that this antibody is specific.

(B) Western blot analysis of RbAp46/48^{LIN-53} using RbAp46/48^{lin-53} mutant strain MT15107 *RbAp46/48^{lin-53} (n3368) I/hT2 [bli-4(e937) let-?(q782) qIs48] (I;III)* (Table S3), in which homozygous deletion was balanced by bli-4- and GFP-marked translocation (Harrison et al., 2006). *RbAp46/48^{lin-53} (n3368)* (a 754 bp deletion) homozygotes were selected by the lack of GFP under fluorescent dissecting microscope, and used for worm lysate preparation. Loss of RbAp46/48^{LIN-53} expression was obvious when compared with N2 wild type. This result suggests that the RbAp46/48^{LIN-53} antibody used in Western (abm SAB494-1) in Fig. 1C is specific.

(C) RBA-1 (64% and 56% nucleotide and amino acid sequence similarity with RbAp46/48^{LIN-53}, respectively) RNAi by soaking (dsRNA is ~65% identical with RbAp46/48^{LIN-53} nucleotide sequence, but with 5% gap) resulted in 100% embryonic lethality, suggesting the depletion by RNAi was efficient. Embryonic lethality was estimated from the average of 3 independent RNAi experiments. Error bars as in Fig. 1B.

(D) Representative live-cell images and quantification of GFP::CENP-A^{HCP-3} signal intensity on mitotic chromosomes in RBA-1 RNAi, relative to wild type. CENP-A^{HCP-3} localization is not affected. Scale bar: 10 μm. Error bars as in Fig. 1B. Despite the similarity between RbAp46/48^{LIN-53} and RBA-1, only RbAp46/48^{LIN-53} affects CENP-A^{HCP-3} localization.

(E) Representative immunofluorescence staining of RbAp46/48^{LIN-53} in wild type embryos and in RBA-1 RNAi. RbAp46/48^{LIN-53} interphase signal was not reduced in RBA-1 RNAi embryos. Scale bar: 5 μm. Quantification of normalized RbAp46/48^{LIN-53} signal intensity in RBA-1 RNAi relative to wild type. Error bars as in Fig. 1B. This, together with Fig. 2A, suggests that the RbAp46/48^{LIN-53} antibody used in immunofluorescence (abcam® ab53616) is specific.

(F) Representative live-cell images and quantification of GFP::M18BP1^{KNL-2} (in OD85 (Table S3)) signal intensity on mitotic chromosomes after RbAp46/48^{LIN-53} RNAi by injection, relative to wild type. Scale bar: 10 μm. Error bars represent standard deviation of the mean. Normal localization of GFP::M18BP1^{KNL-2} in

RbAp46/48^{LIN-53} injection RNAi was consistent with the result by soaking RNAi (Fig. 2C).

(G) Representative live-cell images of ectopic punctate GFP::M18BP1^{KNL-2} foci, which do not overlap with the chromatin (H2B), in RbAp46/48^{LIN-53} soaking RNAi in metaphase. Scale bar: 10 μm. The significance of these ectopic foci is unclear, but these foci were not observed by immunofluorescence (Fig. S2H).

(H) Representative immunofluorescence staining of M18BP1^{KNL-2} in wild type embryos and in RbAp46/48^{LIN-53} soaking RNAi. Scale bar: 5 μm. M18BP1^{KNL-2} localizes to the kinetochore in late prometaphase in RbAp46/48^{LIN-53} soaking RNAi, consistent with the live-cell imaging result in Fig. 2C. No ectopic M18BP1^{KNL-2} was observed by immunofluorescence using anti-M18BP1^{KNL-2} antibody.

S3

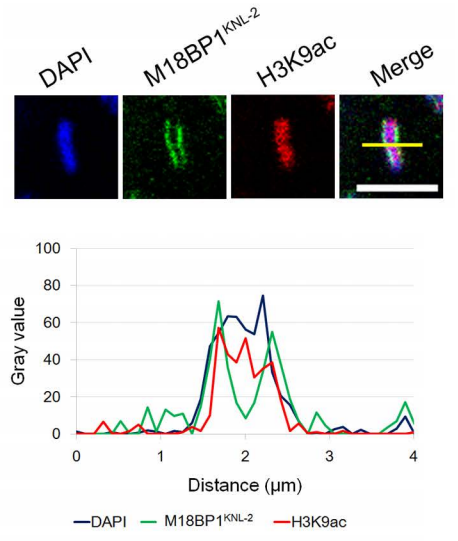
DAPI
M18BP1KNL-2
H3K9ac
Merge
100
80
60
40
20
0
Gray value
0
1
2
3
4
Distance (μm)
DAPI
M18BP1KNL-2
H3K9ac

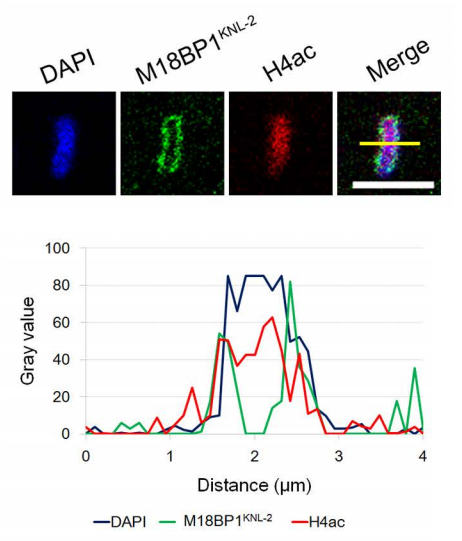
DAPI
M18BP1KNL-2
H4ac
Merge
100
80
60
40
20
0
Gray value
0
1
2
3
4
Distance (μm)
DAPI
M18BP1KNL-2
H4ac

Fig. S3 Histone H3 and H4 are not specifically hypoacetylated at the kinetochore, related to Fig. 3

Representative immunofluorescence images of M18BP1^{KNL-2}, H3K9ac, H4ac and DAPI on metaphase chromosomes in wild type embryos. Scale bar: 5 μm. Line scan analysis of the signal intensity, showing that H3K9ac and H4ac span the whole metaphase plate, and are not hypoacetylated at poleward faces.

S4A

RbAp46/48^{LIN-53}-containing complexes' core component	**Reported phenotype upon RNAi**	**Observed phenotype upon RNAi**
HAT-1$^{TAG-235}$	>10% embryonic lethal (Maeda et al., 2001)	9±3.34% (n=3) embryonic lethal
CHD4$^{LET-418}$	Larval Arrest at Early L1/L2 (Sonnichsen et al., 2005)	100±0.53% (n=3) arrest at early larval stage
NURF301^{NURF-1}	Suppress SynMuv of *lin-53(n833); lin-15A(n767)* (Andersen et al., 2006)	Suppress Muv from 71% (n=24) to 46% (n=13)
CHAF-1 (p150)	100% embryonic lethal (Sonnichsen et al., 2005)	100±0% (n=3) embryonic lethal
SIN-3	Suppress SynMuv of MT664 *lin-8(n111) II; lin-15B (n374) X* (Cui et al., 2006)	Suppress Muv from 68% (n=23) to 41% (n=20)
LIN-54	Up to 50% of the F1 adults show protruding vulva (Sonnichsen et al., 2005)	48±1.77% (n=3) of the F1 adults have protruding vulva

S4B

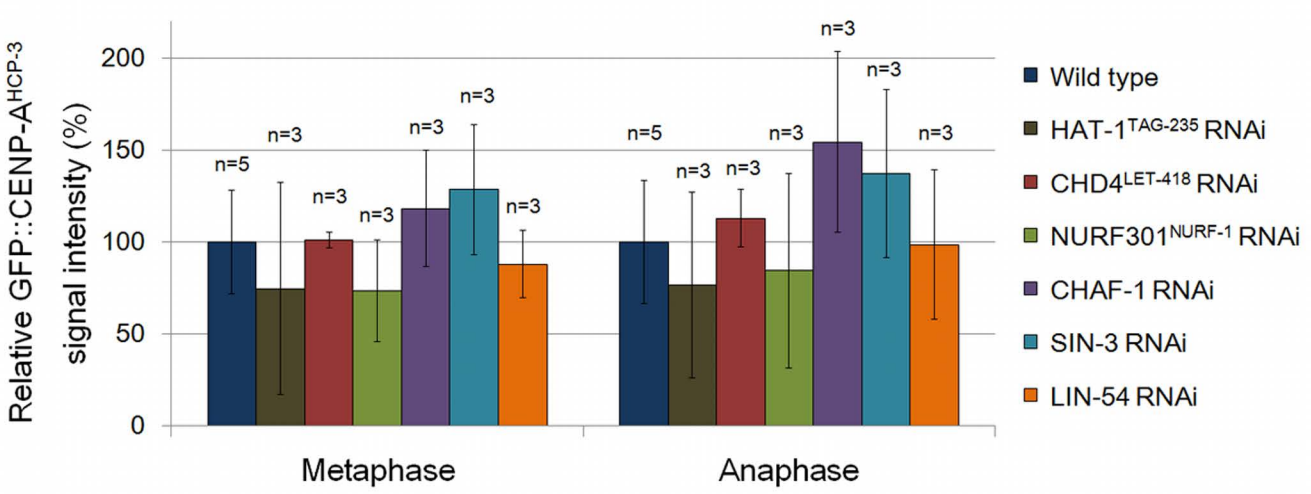

Fig. S4 Verification of the 6 complex RNAi efficiency and effects on GFP::CENP-A^{HCP-3} localization, related to Fig. 4

(A) Table showing published RNAi phenotypes, and phenotypes observed after injection RNAi of the core components of the 6 complexes tested, suggesting the RNAi depletions were efficient. Average percentage and standard deviation of the mean was indicated.

(B) Quantification of GFP::CENP-A^{HCP-3} (in OD421) signal intensity on mitotic chromosomes after injection RNAi of the core components of the 6 complexes. None of them recapitulated the delocalization of CENP-A^{HCP-3} as in RbAp46/48^{LIN-53} RNAi, consistent with the results by soaking RNAi (Fig. 4B), suggesting RbAp46/48^{LIN-53} may function independently of these complexes.

Supplemental Tables

Table S1. Proteins identified by CENP-A^{HCP-3} IP-MS, related to Figure 1.
Thirty-five proteins, including CENP-A^{HCP-3} itself and RbAp46/48^{LIN-53}, were isolated by both anti-CENP-A^{HCP-3} antibodies OD79 and SDQ0804 (with total sequence coverage >=30%), but not by anti-GST antibody.

Gene name	Sequence coverage (%)		Function
	OD79	SDQ0804	
rla-2	85.5	85.5	Acidic ribosomal subunit protein P2
act-4	58.6	69.3	Actin isoform
Y69A2AR.18a	46.8	26.4	Ortholog of human ATP5C1
rps-0	46.4	34.8	Small ribosomal subunit SA protein
rpl-31	43.4	27.9	Large ribosomal subunit L31 protein
rpl-25.2	42.5	27.4	Large ribosomal subunit L23a protein
rps-23	37.8	27.3	Small ribosomal subunit S23 protein
rps-1	37.7	18.3	Small ribosomal subunit S3A protein
prdx-2	34.4	12.3	2-Cys peroxiredoxin, peroxidase enzyme
rpl-9	33.9	19	Large ribosomal subunit L9 protein
hda-1	33.6	51.4	Histone deacetylase 1
inf-1	31.3	11.7	Similar to eukaryotic initiation factor 4A
cpl-1	31.2	22.8	Member of the cathepsin L-like cysteine protease family
ndk-1	30.1	30.1	Nucleoside Diphosphate Kinase
rpl-12	29.7	29.7	Large ribosomal subunit L12 protein
hcp-3	**29.5**	**19.8**	**Centromere protein (CENP)-A homolog required for kinetochore function**
fkb-2	28.7	39.8	Peptidylprolyl cis/trans isomerase homologous to the mammalian FKBP1A
rpt-2	28.4	22.3	Ortholog of human PSMC1
rps-5	27.1	22.9	Small ribosomal subunit S5 protein
rpn-2	26.6	30.6	Non-ATPase subunit of the 26S proteasome's 19S regulatory particle (RP) base subcomplex
mbd-2	25.2	22.9	Truncated ortholog of methyl-CpG-binding-domain (MBD) proteins
F23C8.5	25.1	22.4	Ortholog of human electron transfer

			flavoprotein beta subunit (ETFB)
rpt-3	23.4	34.1	Triple A ATPase subunit of the 26S proteasome's 19S regulatory particle (RP) base subcomplex
rpl-13	23.2	12.1	Large ribosomal subunit L13 protein
rpl-11.1	21.9	24.5	Large ribosomal subunit L11 protein
vit-4	21.3	26	Predicted lipid transporter
cct-7	21.3	21.9	Putative eta subunit of the eukaryotic cytosolic 'T complex' chaperonin
rps-10	20.1	20.1	Small (40S) ribosomal subunit S10 protein
acca-2	17.5	20.1	Ortholog of human ACAA2
aldo-2	17.5	15.6	Fructose-bisphosphate aldolase
rpt-5	15.8	33	Triple A ATPase subunit of the 26S proteasome's 19S regulatory particle (RP) base subcomplex
lin-53	**15.3**	**37.4**	**Class B synMuv protein similar to the mammalian homolog RbAp46/48**
rpl-30	13.3	32.7	Large ribosomal subunit L30 protein
let-418	4.2	30.1	Homolog of Mi-2/CHD3, a component of the NURD complex
lin-40	4.5	34	Homolog of human MTA1, part of NURD complex

Table S2. Primers used for dsRNA production, related to Experimental Procedures.

Targeted gene	Forward/ Reverse	Sequence (5' to 3')
hcp-3	Forward	GCAAAATGAGAGCGTCACAA
	Reverse	TCAGAGATGTCGAAGGCAGA
knl-2	Forward	TCGACTTGGTCGGACAGATT
	Reverse	TGCGATATGTGGCGTTATGT
lin-53	Forward	CCCCGTTCTTGTACGATCTC
	Reverse	GGCAGATTGGTCTTCTCCAA
tba-1	Forward	CCGATACTGGAAACGGAAGA
	Reverse	CAGTGTTGACGTCCTTTGGA
his-9	Forward	TCGTACTAAGCAAACCGCCC
	Reverse	TTAAGCACGCTCTCCTCGGA
his-10	Forward	GGACGTGGAAAGGGAGGAAA
	Reverse	ATCCTCCGAATCCGTACAGG
rba-1	Forward	CAATGGATGCCTGATGTCAC
	Reverse	GCATTAAATTCGTCGCTGCT
mes-2	Forward	TCCAATCGAGCAAAGTGTGG
	Reverse	TTTCCGCATCCAGACCATCT
tag-235	Forward	TCACACAGCTCAAACCCTCT
	Reverse	GGTGCATACAACCGACGTTT
let-418	Forward	CTAAGCTCGTTCAAGGTGGC
	Reverse	TCGTCAACAGGAGCGTTTTG
nurf-1	Forward	GGCGGATTGACTATGCAAAT
	Reverse	TCCGAAGTACGACGCTCTTT
chaf-1	Forward	CAACAGTCCCCAAAAGCTCC
	Reverse	TCTTCCTCACCACCATCGTC
sin-3	Forward	ATGGAGAGACGCTTTGGACA
	Reverse	CTTGACGGCTTCCTCGAATG
lin-54	Forward	ACTTACAGGCGCAGCAAAAT
	Reverse	CCATCTCGACCTTCGGTTTA

Table S3. Worm strains used and their genotypes, related to Experimental Procedures.

Strain	Genotype	Reference
N2	Wild type	
OD421	*unc-119(ed3) III; ltSi4 [pOD833; hcp-3p/GFP::hcp-3; cb unc-119(+)] II; hcp-3(ok1892) III; ltIs37[pAA64; pie-1p/mCherry::his-58; unc-119 (+)]*	(Gassmann et al., 2012)
AV221	*unc-119(ed3) meT8 (III); meIs4 [lacOp/rol-6(su1006)::lacO] meT8 (IV); mels1 [pie-1p/GFP::lacI; unc-119(+)]*	(Bilgir et al., 2013)
OD85	*unc-119(ed3) III; ltIs37 [pAA64; pie-1p/mCherry::his-58; unc-119 (+)]; ltIs22 [pPM3; pie-1p/GFP-TEV-STag::knl-2; unc-119(+)].*	(Maddox et al., 2007)
OD143	*unc-119(ed3) III; ltIs114 [pJM1; pie-1p:: GFP::CENP-AHCP-3; unc-119 (+)]; ltIs37 [pAA64; pie-1p::mCHERRY::his-58(H2B); unc-119 (+)] IV*	(Monen et al., 2005)
WYY26	*hkuSi7 [pOD833; hcp-3p::GFP::CENP-A^{HCP-3}; cb unc-119(+)] II*	This study
MT15107	*RbAp46/48lin-53 (n3368) I/hT2 [bli-4(e937) let-?(q782) qIs48] (I;III)*	(Harrison et al., 2006)
MT10408	*in-53(n833) I; unc-76(e911) V; lin-15A(n767) X; nEx998 [lin-53::GFP + unc-76(+)]*	Lu and Horvitz (through CGC)
MT10410	*Lin-53(n844) I; unc-76(e911) V; lin-15(n767) X; nls119 [GFP::lin-53]*	Lu and Horvitz

Supplemental Video

Video S1. Live-cell imaging of OD421 one-cell embryos expressing GFP::CENP-A^{HCP-3} and mCherry::H2B, related to Figure 1.

Images were analyzed by time-lapse confocal microscopy using a spinning disk confocal microscope (PerkinElmer Inc.) with 25 sec frame intervals. GFP::CENP-A^{HCP-3} in green and mCherry::H2B in red. The videos are displayed at 7 frames per second.

(A) In mock treatment.
(B) After CENP-A^{HCP-3} RNAi.
(C) After M18BP1^{KNL-2} RNAi.
(D) After RbAp46/48^{LIN-53} RNAi.

Supplemental Experimental Procedures

Immunoprecipitation and mass spectrometry, related to Table S1

N2 wild type embryo extracts were grinded and treated with micrococcal nuclease (MNase) to release nucleosomes. The chromatin fraction was purified by high-speed centrifugation. Immunoprecipitation was performed using two different anti-CENP-A^{HCP-3} antibodies (OD79, a gift from Arshad Desai and Novus 29540002 SDQ0804), followed by multidimensional protein identification technology (MudPIT). Control IP-MS using anti-GST antibody was performed in parallel to detect non-specific binding proteins.

RNA interference by injection, related to Figure S1, 2 and 4

L4 hermaphrodites were injected dsRNA solution, and recovered at 20°C for 48 h before analysis.

Supplemental References

BILGIR, C., DOMBECKI, C. R., CHEN, P. F., VILLENEUVE, A. M. & NABESHIMA, K. 2013. Assembly of the Synaptonemal Complex is a Highly Temperature-Sensitive Process that is Supported by PGL-1 during Caenorhabditis elegans Meiosis. *G3 (Bethesda)*.

GASSMANN, R., RECHTSTEINER, A., YUEN, K. W., MUROYAMA, A., EGELHOFER, T., GAYDOS, L., BARRON, F., MADDOX, P., ESSEX, A., MONEN, J., ERCAN, S., LIEB, J. D., OEGEMA, K., STROME, S. & DESAI, A. 2012. An inverse relationship to germline transcription defines centromeric chromatin in C. elegans. *Nature,* 484**,** 534-7.

HARRISON, M. M., CEOL, C. J., LU, X. & HORVITZ, H. R. 2006. Some C. elegans class B synthetic multivulva proteins encode a conserved LIN-35 Rb-containing complex distinct from a NuRD-like complex. *Proc Natl Acad Sci U S A,* 103**,** 16782-7.

MADDOX, P. S., HYNDMAN, F., MONEN, J., OEGEMA, K. & DESAI, A. 2007. Functional genomics identifies a Myb domain-containing protein family required for assembly of CENP-A chromatin. *J Cell Biol,* 176**,** 757-63.

MONEN, J., MADDOX, P. S., HYNDMAN, F., OEGEMA, K. & DESAI, A. 2005. Differential role of CENP-A in the segregation of holocentric C. elegans chromosomes during meiosis and mitosis. *Nat Cell Biol,* 7**,** 1248-55.